CONTRACT REPORT ARBRL-CR-00507

COMBUSTION OF NITRAMINE PROPELLANTS

Prepared by

Princeton Combustion Research Laboratories
1041 U. S. Highway One North
Princeton, NJ 08540

March 1983

US ARMY ARMAMENT RESEARCH AND DEVELOPMENT COMMAND
BALLISTIC RESEARCH LABORATORY
ABERDEEN PROVING GROUND, MARYLAND

Destroy this report when it is no longer needed.
Do not return it to the originator.

Additional copies of this report may be obtained
from the National Technical Information Service,
U. S. Department of Commerce, Springfield, Virginia
22161.

The findings in this report are not to be construed as
an official Department of the Army position, unless
so designated by other authorized documents.

REPORT DOCUMENTATION PAGE		READ INSTRUCTIONS BEFORE COMPLETING FORM
1. REPORT NUMBER CONTRACT REPORT ARBRL-CR-00507	2. GOVT ACCESSION NO.	3. RECIPIENT'S CATALOG NUMBER
4. TITLE (and Subtitle) COMBUSTION OF NITRAMINE PROPELLANTS		5. TYPE OF REPORT & PERIOD COVERED Final Report 6. PERFORMING ORG. REPORT NUMBER PCRL-FR-82-003
7. AUTHOR(s) Moshe Ben-Reuven and Martin Summerfield		8. CONTRACT OR GRANT NUMBER(s) DAAK11-80-C-0104 AFOSR-MIPR-81-00004
9. PERFORMING ORGANIZATION NAME AND ADDRESS Princeton Combustion Research Laboratories 1041 U.S. Highway One North Princeton, NJ 08540		10. PROGRAM ELEMENT, PROJECT, TASK AREA & WORK UNIT NUMBERS 1L161102AH60
11. CONTROLLING OFFICE NAME AND ADDRESS US Army Armament Research & Development Command US Army Ballistic Research Laboratory (DRDAR-BLA-S) Aberdeen Proving Ground, MD 21005		12. REPORT DATE March 1983 13 NUMBER OF PAGES 99
14. MONITORING AGENCY NAME & ADDRESS(if different from Controlling Office)		15. SECURITY CLASS. (of this report) UNCLASSIFIED 15a. DECLASSIFICATION/DOWNGRADING SCHEDULE

16. DISTRIBUTION STATEMENT (of this Report)

Approved for public release; distribution unlimited.

17. DISTRIBUTION STATEMENT (of the abstract entered in Block 20, if different from Report)

18. SUPPLEMENTARY NOTES

19. KEY WORDS (Continue on reverse side if necessary and identify by block number)

monopropellant combustion; composite propellant combustion; nitramine deflagration; melt phase decomposition; combustion modeling; numerical analysis; steady state burning

20. ABSTRACT (Continue on reverse side if necessary and identify by block number)

The objective of this study is to improve the physical understanding of cyclic nitramine (RDX, HMX) combustion, through development of a comprehensive analytical model. The ultimate goals are to enable prediction of deflagration rate over a wide pressure range (7-70 MPa), its pressure and temperature sensitivities, and indicate effective means by which the burning rate can be modified or tailored.

DD FORM 1473 1 JAN 73   EDITION OF 1 NOV 65 IS OBSOLETE

The analysis is divided into 2 major parts: (1) critical review of existing nitramine combustion models, in particular, the Beckstead-Derr-Price (BDP) approach. Particular deficiencies in this analysis were pointed out, and an improved approximate model was derived; simulation of available HMX (and AP) burn rate data were performed with both models for comparison. Although the latter model is clearly superior in burn rate prediction, both simple models fail in correlating existing temperature-sensitivity data. (2) In the second part, a comprehensive deflagration model is derived, incorporating the following elements: nonequilibrium evaporation law at the melt/gas interface, serving as an auxiliary condition to enable independent burn rate prediction; improved melt phase model including decomposition-gas bubbles; model for far-field processes, with several simultaneous secondary reactions. Results from the bubbly-melt phase integration are shown. The solutions show that for given (m, T_s) data, the extent of subsurface decomposition decreases appreciably, while the heat feedback to the surface increases, relative to the results of the model excluding bubbles.

TABLE OF CONTENTS

LIST OF FIGURES

INTRODUCTION

Development of nitramines as solid propellant ingredients has identified the sketchy understanding of their combustion mechanisms. The chemistry and hydrodynamics have yet to be satisfactorily combined to give a description of how the combustion process could be controlled or modified. Present developments rely on trial-and-error empiricism in adopting formulations and predicting their response to variations in pressure, initial temperature, gas velocity, and composition. Improvements are needed in the theoretical description of the combustion process. A model, developed at Princeton University, forms the basis for improvements.

The objective, in general, is to improve the theoretical description of nitramine propellant combustion, through development of a comprehensive model. More precisely, this is to be accomplished through the following tasks:

(1)   Devise an improved physical model for the vaporization and liquid layer of a nitramine monopropellant. Use the improved model to compute regression rate dependence on pressure and initial temperature over the pressure range 7-70 MPa and temperature range 230-330 K.

(2)   Devise an improved submodel for the liquid layer accounting for bubbles. Use the improved model to calculate combustion solutions to be compared with earlier published solutions at 1-4 MPa.

(3)   Perform a critical review of other combustion models of monopropellant and of nitramine based composite propellant.

(4)   Perform a critical analysis of the effect of the three chemical reactions used in the existing monopropellant model with a view to a scheme to catalyze the reactions.

(5)   Collect and analyze available data on nitramine monopropellant combustion with a view to suggesting which data should be considered baseline for model validation.

Items (3) and (5) are performed in Section 2, and items (1) and (2) in Section (3) herein. Task (4) is still incomplete at the time of this writing; an effort is made to conclude this study in the near future.

I. CRITIQUE OF THE BECKSTEAD-DERR-PRICE (BDP) PROPELLANT COMBUSTION MODEL

1.1 Background

Over a decade ago, Beckstead, Derr and C.F. Price introduced a model of solid monopropellant and propellant combustion [1,2], referred to as BDP herein. The corresponding flame structure postulated is depicted in Fig. 1, where the overall physical concept is shown. It consists, for each oxidizer crystal exposed at the surface, of three types of gaseous flames. As will be discussed later, each of these flames is assumed to contribute a component of heat feedback proportional to $\exp(-z_i)$ where z_i (i = 1, 2, 3) denote dimensionless "flame standoff" distances. The BDP approach was used widely in the U.S. ever since, and was applied to a rather diverse propellant lot, including ammonium perchlorate composites, composite-modified double base, and nitramine (HMX, RDX) propellants. Interestingly, a previous composite propellant combustion model, the granular diffusion flame (GDF) model of Summerfield [3,4,5] was far less accepted in comparison, despite its considerable success in simulation of burning rate pressure-dependence for a large class of ammonium perchlorate composites [6]. The GDF model was criticized for its intuitive formulation, [7,8] based on dimensional or physical scaling arguments, rather than formal derivation; its success in burning rate simulation was attributed to the availability of two adjustable constants.

An appreciable number of well-developed composite propellant combustion models has been reported over the past decade, which endeavored to incorporate many real-life effects, such as propellant structure, energetic binder and aluminized configurations. Such are the works of Beckstead [9-13], Cohen [14-17], King [18,19], and the statistical refinements by Glick [20-23], all of which had evolved from the original BDP model of 1970. In most cases, good comparisons with experimental burning rate vs pressure were obtained. Surprisingly, the gas phase combustion effects are still in the $\exp(-z_i)$ form.

In contrast to the highly approximate treatment of combustion processes in all of the BDP-type models, the following aspects assume great relative importance: propellant matrix structure, oxidizer particle sizes and distributions, and surface structure (e.g., convex or concave burning oxidizer surfaces, appearance of melt layers). This is not to say, unfortunately, that these structural elements have been rigorously treated. To the contrary, their representation and relevance to the burning process can be inferred only speculatively at present. Indeed, the incorporation of these properties gave rise to a large number of adjustable constants in the formulation, which can not be derived analytically nor verified by physical measurements.

To obtain some preliminary insight into the development of BDP modeling over the years, the following calculation is carried out, cum granu salis. Regarding the surface energy balance (the centerpiece of all BDP models), the symbols denoting combustion effects (i.e., the exponential terms), and the totality of right-hand side symbols (gas phase heat feedback) are enumerated; their ratio (the so-called combustion fraction) represents a point in Fig. 2 for each investigation. The resultant decaying linear trend obtained by least-squares fit demonstrates that the relative importance of combustion in solid propellant regression is diminishing in time and may even vanish during the 1980s. One may envision the Space Shuttle boost phase in 1990 powered entirely by oxidizer granularity, modality and volume fraction.

The foregoing trend should be envied by other combustion system models, but deserves closer examination: Is the exponential combustion term, as stated by BDP, consistent with modern combustion theory, available since the 1950s? Are the physical and analytical BDP models compatible with their own physical picture, as depicted in Fig. 3? These are some of the questions which motivate the present critique. More precisely, regarding Fig. 3, the questions posed for this analysis are: (1) Is the monopropellant flame properly formulated mathematically? (2) Can the heat feedback contributions from the various "adiabatic" flame components be simply superimposed, without interaction? (3) Can a planar flame sheet at a mean standoff distance represent a conical or parabolic diffusion flame surface? (4) Is this parabolic flame surface truly diffusion controlled? The approach is simply to check the validity of the BDP combustion model within the framework of its own physical picture or basic assumptions. This is carried out in a constructive manner, with parallel derivations offered which are in agreement with present knowledge of combustion theory and implement available thermochemical data.

9

1.2 The Monopropellant (Oxidizer) Flame

The basis for the heat feedback expression in the BDP monopropellant analysis [1,2], viz,

$$dr/dz(0^+) = e^{-z_B} \tag{1}$$

is an approximation of the single (overall) exothermic chemical reaction step in the gas phase by a Dirac delta function, at a dimensionless standoff distance

$$z_B \equiv y_1^*/(\lambda/mc_p) \tag{2}$$

The energy interface condition (at $z = 0^+$) corresponding to Eq. (1) as used by BDP is

$$dr/dz(0^+) = q \equiv \left[c_c(T_s-T_0) - Q_s^* \right]/Q_f^* \tag{3}$$

where the dimensionless thermal enthalpy is $\tau = C_p(T-T_s)/Q_f^*$, Q_s^* is the net surface heat release, and Q_f^* is the net gas phase exothermicity. The result of Eq. (1) obviously pertains to the solution of the homogeneous energy equation $\tau'-\tau'' = 0$ for the region $0 < z < z_B$. This strictly precludes the effect of chemical reaction and necessitates extraneous introduction of chemical kinetics effects through the intuitive standoff approximation $y_1^* = m/\Omega$, proposed earlier by Hermance [24]. Thus, Eq. (2) yields

$$z_B = m^2/\left(\frac{\lambda}{C_p}\right)\Omega(p,T_f) \tag{4}$$

where m is the mass flux and Ω denotes the mean reaction rate.

Alternative derivation (MFR)

The use of this extraneous condition can be entirely avoided when a more rigorous analysis (still within the delta function approximation framework) is carried out, as follows. Consider the following simplified chemical reaction scheme:

SUBSURFACE DECOMPOSITION:	$R(c) \rightarrow P(g) + Q_c$	(5.a)
VAPORIZATION @ SURFACE:	$R(c) \rightarrow R(g) + Q_v$	(5.b)
GAS PHASE REACTION	$R(g) \rightarrow P(g) + Q_1$	(5.c)

10
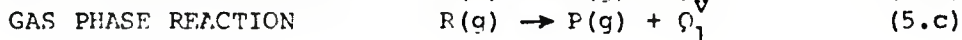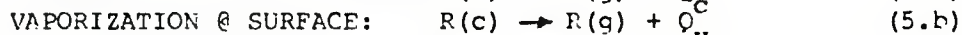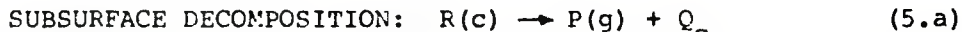
R and P denote reactant and product mixtures, respectively.
$Q_c = Q_l + Q_v$ is the net heat of reaction in the condensed phase,
and vaporization in step (5b) can be either simple phase change or
dissociative. Note: $Q > 0$ denotes exothermicity herein. The physical
model for the delta function flame is shown in Fig. 4.

The dimensionless conservation equations in the gas phase, for
$0 < z < \infty$ are

$$-d^2\theta/dz^2 + d\theta/dz = \Lambda\,\delta(z-z_1) \qquad (6.a)$$

$$-d^2Y/dz^2 + dY/dz = -\Lambda\,\delta(z-z_1) \qquad (6.b)$$

where $\theta \equiv C_p(T-T_s)/Q_1^*$ and Y denote reduced thermal enthalpy and a
reference (consumable) species mass fraction, respectively. The flame
speed eigenvalue is defined:

$$\Lambda \equiv \frac{\lambda}{C_p}\,\Omega(p,T_f)/m^2 \qquad (7)$$

with Ω being the mean reaction rate. The boundary data are

$$\theta(0^+) = 0, \quad d\theta/dz(0^+) = q_0, \quad \theta(\infty) = \theta_f \qquad (8)$$

$$Y(0^+) - dY/dz(0^+) = G \qquad (9.a)$$

$$Y(\infty) = dY/dz(\infty) = 0 \qquad (9.b)$$

where $\theta_f \equiv C_p(T_f - T_s)/Q_1^*$ and

$$q_0 = [\,C_c(T_s - T_0) - Q_s^*\,]/Q_1^* \qquad (10)$$

Using an integrating factor, the solution of the differential system,
Eqs. (6)-(9) is readily found

$$\theta(z) = q_0(e^z - 1) - \Lambda(e^{z-z_1} - 1)\cdot 1(z-z_1) \qquad (11.a)$$

where $1(z-z_1)$ is the Heaviside (or unit step) function; a similar
solution obtains for the species equation. A single integration of
Eq. (6.b) between 0 and infinity is facilitated by the delta function
imposed. This yields, after implementation of Eqs. (9.a,b):

$$\Lambda = G \qquad (11.b)$$

11

where G is the total incoming flux of reactant 'R,' available at the surface. Note that G <1 whenever subsurface decomposition prevails. The net surface heat release is, cf Eqs. (5a,b,c):

$$Q_s^* = Q_m^* + (1-G)Q_c^* + GQ_v^*$$

(12)

Note that all subsurface heat release assumed to occur at the surface, and the total gas phase heat release is

(13)

In general, the extent of subsurface decomposition depends on surface temperature, residence time and other parameters: $G = G (T_s, m; T_o)$ can be written. Hence G may be variable; this has not been recognized in the BDP model, which precludes any consideration of chemical species.

The heat feedback, obtained from a single integral of Eq. (6.a), using an integrating factor:

$$d\Theta/dz(0^+) = \Lambda e^{-z_1}$$

(14)

is formally similar to that of BDP, cf Eq. (1). However, the central issue of the present derivation as regards burning rate calculation, is the flame speed eigenvalue,

$$\frac{\lambda}{C_p} \Omega(P,T_f)/m^2 = G$$

(15)

combining Eqs. (7) and (11), which naturally incorporates the subsurface processes along with the effect of gas phase chemical kinetics.

The mean reaction rate in Eq. (15) can be put more explicitly,

$$\Omega(P,T_f) = K_1 e^{-\beta_1/T_f} p^{n_1}$$

(16)

where n_1 and β_1 denote the overall reaction apparent order and activation energy, respectively, while K_1 is proportional to the prefactor. Substitution in Eq. (15) yields

$$m = \left[\frac{\lambda}{C_p} K_1 e^{-\beta_1/T_f} p^{n_1}/G(T_s,m;T_0) \right]^{1/2}$$

(17)

12

The BDP analysis obtains an analogous expression, using the heat feedback expression, Eqs. (1), (3) and (4):

$$m(BDP) = \left[\frac{\lambda}{C_p} k_1 e^{-\beta_1/T_f} p^{n_1} \cdot \ell u \left(\frac{1}{q} \right) \right]^{1/2} \quad (18)$$

Comparison between the burning rate expressions, Eqs. (17,18), reveals a fundamental difference, demonstrated by the following simple test case. Whenever $G(T_s, m; T_o)$ = const, and T_f = const, the region $0 < z < \infty$ is equivalent to the same region in a pure gaseous deflagration (subject to the same delta function approximation, of course), regardless of "surface temperature" variation.

In this instance, $m \sim p^{n_1/2}$ is expected, as indeed given by Eq. (17) derived herein, but not from the analogous BDP expression, Eq. (18), where an explicit T_s-dependence prevails; this dependence indicates inconsistency with the physics of the problem.

Note that the validity of the foregoing equivalence argument (with pure gaseous deflagration) can be readily established mathematically by noting that G = const implies (letting $C_c = C_p$ for this purpose)

$$\theta_f(T_s) + q_0(T_s) = \Lambda = const \quad (19)$$

as obtained by integration of Eq. (6.a) once, and using Eqs. (8); this is compatible with the overall enthalpy balance. Consequently, a manifold of genuine solutions can still be generated for distinct values of T_s, as long as the linear combination of Eq. (19) is maintained, each solution with a distinct burning rate (or flame speed), despite the eigenvalue Λ being fixed.

It should be pointed out that the delta function flame treatment herein is quite crude, and was intended only to simulate the physical model used by BDP. Contrary to popular legend, propagated by an erroneous footnote in the KTSS paper [25], this approach was never initiated by von Karman;* it was used by Zeldovich in a simplified treatment of chain reactions [27]. There exist much more rigorous analytical treatments of gaseous deflagrations, using matched asymptotic expansions, by Jain and Kumar [28], Bush and Fendell [29], Joulin and Clavin [30] and Ben-Reuven [31].

To obtain formal closure, by which the burning rate, m, could be calculated, both formulations require a pyrolysis law, or $m = m(T_s)$; in addition, Eq. (17) requires also explicit knowledge of subsurface processes, to obtain explicitly $G(T_s, m; T_o)$. Once

---

* in particular, no mention of such approximation was made in the classical von Karman paper given at the Sixth International Combustion Symposium in 1956 [26].

13

closure is obtained, the burning rate pressure sensitivity and the temperature sensitivity can be derived for both models. In general, these properties are defined,

$$n \equiv \left. \frac{\delta m/m}{\delta P/P} \right|_{T_0} , \qquad \sigma_P \equiv \left. \frac{\delta m/m}{\delta T_0} \right|_P \qquad (20)$$

where δ here denotes the variational operator.

From Eq. (17), the first variation leads to

$$\frac{\delta G}{G} + 2 \frac{\delta m}{m} = n_1 \frac{\delta P}{P} + \frac{\delta \overline{K}}{\overline{K}} \qquad (21)$$

where

$$\overline{K}(T_f) \equiv \frac{\lambda}{C_P} K_1 e^{-\beta_1/T_f} , \qquad K_1 \equiv A_1 T^{\alpha_1}/(R_u T)^{n_1} \qquad (22)$$

Note that we assume that the product $(\lambda/C_p) K_1$ is independent of temperature for any reaction order n_1 under consideration. Now,

$$\frac{\delta G}{G} = \left[\frac{\partial \ln G}{\partial T_s} \cdot \frac{\partial T_s}{\partial \ln m} + \frac{\partial \ln G}{\partial \ln m} \right] \frac{\delta m}{m} + \frac{\partial \ln G}{\partial T_0} \cdot \delta T_0 \qquad (23.a)$$

$$\frac{\delta \overline{K}}{\overline{K}} = \left[\frac{\partial \ln \overline{K}}{\partial T_f} \cdot \frac{\partial T_f}{\partial T_s} \cdot \frac{\partial T_s}{\partial \ln m} \right] \frac{\delta m}{m} + \frac{\partial \ln \overline{K}}{\partial T_f} \cdot \frac{\partial T_f}{\partial T_0} \delta T_0 \qquad (23.b)$$

The algebraic sum of all $\delta m/m$-terms, collected:

$$a \equiv \frac{\partial \ln G}{\partial T_s} \cdot \frac{\partial T_s}{\partial \ln m} + \frac{\partial \ln G}{\partial \ln m} - \frac{\partial \ln \overline{K}}{\partial T_f} \cdot \frac{\partial T_f}{\partial T_s} \cdot \frac{\partial T_s}{\partial \ln m} + 2 \qquad (23.c)$$

Thus, using Eqs. (20), (21) and (23):

$$n(MBR) = n_1/a \qquad (24.a)$$

$$\sigma_P(MBR) = \left(\frac{\partial \ln \overline{K}}{\partial T_f} \cdot \frac{\partial T_f}{\partial T_0} - \frac{\partial \ln G}{\partial T_0} \right)/a \qquad (24.b)$$

which still require explicit definition of $G(T_s, m; T_0)$. In comparison, the corresponding BDP-derived sensitivities can be written explicitly,

$$n(BDP) = n_1 / \left[2 + C_P T_s^2/\beta_1 Q_f^* z_B e^{-z_B} \right] \qquad (25.a)$$

14

$$\dot{Q}_p(BDP) = \frac{\beta_1/T_f^2 + C_p/Q_f^* z_B e^{-z_B}}{2 + C_p T_s^2/\beta_1 Q_f^* z_B e^{-z_B}} \qquad (25.b)$$

where, cf Eqs. (1),(3),

$$z_B = \ln[1/q(T_s)] = \ln\left[\frac{Q_f^*}{C_c(T_s-T_o)-Q_s^*}\right]$$

Note that $C_c = C_p$ is assumed in the original BDP formulation, whereby T_f is formally independent of T_s.

Evidently, the actual values obtained by Eqs. (24.a,b) herein depend on the particular subsurface processes, whereby $G = G(T_s, m; T_0)$ is defined, which is expected to differ from one monopropellant type to another. In contrast, the sensitivities obtained from the BDP formulation, Eqs. (25.a,b), depend only on a suitable choice of the parameter family, $(E_1, Q_f^*, Q_s^*, ...)$, while the underlying functional dependences remain fixed for all monopropellant types. This is a rather strong statement, regarding the universality of monopropellant decomposition and combustion mechanisms, totally unwarranted by the physical processes involved. The foregoing statement does not detract, however, from the simulative capabilities of the function

$$f_B(T_s) \equiv T_s^2/z_B\, e^{-z_B} \qquad (26)$$

which appears in the denominator of Eqs. (25.a,b). As will be demonstrated later, f_B has a remarkable correlative power.

To facilitate comparison with the BDP model, two highly simplifed cases are constructed, as follows.

(1) For AP simulation,

$$G(T_s, m) = 0.3 = \text{const}, \quad @ \; T_0 = 300\,K \qquad (27.a)$$

i.e., 70% of AP decomposition is assumed to occur with the subsurface region, in line with similar considerations by BDP, and, in a much more detailed AP deflagration model, by Guirao and Williams [32]. In addition, $C_c > C_p$ is assumed herein, leading to an explicit dependence of the adiabatic flame temperature, T_f, on T_s through the overall enthalpy balance:

$$C_c(T_s-T_o) + C_p(T_f-T_s) = Q_m^* + Q_v^* + Q_1^* \qquad (27.b)$$

whereby,

$$(\partial T_f/\partial T_s)_{T_0} = (C_p - C_c)/C_p \qquad (27.c)$$

Note that although $(C_c - C_p)T_s/Q_1^*$ is expected to be small, still $(C_c - C_p)/C_p \sim \mathbf{O}(1)$ according to available data.

15

It should be pointed out that $\delta G = 0$ at $\delta T_0 = 0$, while δT_s, δm, $\delta p \neq 0$, may still follow from the general case outlined in Eq. (23.a):

$$\frac{\partial \ln G}{\partial T_s} \cdot \frac{\partial T_s}{\partial \ln m} + \frac{\partial \ln G}{\partial \ln m} = 0.$$

This implies that residence time and characteristic chemical kinetics relaxation time in the subsurface region balance exactly to yield zero variation of G under these conditions. However, for $\delta T_0 \neq 0$, while $\delta p = 0$ and δT_s, $\delta m \neq 0$, one may have

$$\frac{\delta G}{G} = \frac{\partial \ln G}{\partial T_0} \delta T_0 \neq 0$$

from Eq. (23.a). The corresponding correction to the temperature sensitivity in this particular case is derived in the second part of Appendix A.

(2) For nitramine simulation (HMX in particular), the extent of subsurface decomposition expected is much smaller in comparison, but variable. The following approximation is based on the assumption that the activation energy, F_c, is high, and hence most of the first-order overall reaction in the liquid phase occurs in a thin region near the surface. For the derivation given in Appendix A, the result is

$$G(T_s, m; T_0) \doteq \exp\left[-K_c e^{-1/\varepsilon} \varepsilon \frac{T_s}{T_s - T_0}\right] \qquad (28.a)$$

$$K_c \equiv \lambda_c \rho_c A_c / C_c m^2 , \quad 0 < \varepsilon \equiv T_s / \beta_c \ll 1 \qquad (28.b)$$

The appropriate partial derivatives are

$$\left. \begin{aligned} \partial \ln G / \partial T_s &= \ln G \left[\frac{1}{\varepsilon} + \frac{T_s - 2T_0}{T_s - T_0}\right] / T_s \\ \partial \ln G / \partial m &= -2 \ln G / m \\ \partial \ln G / \partial T_0 &= \ln G / (T_s - T_0) \end{aligned} \right\} \qquad (28.c)$$

Further, in this case, $C_c \doteq C_p$ is considered in good agreement with measured C_c and calculated C_p (gas phase near-field) data.

In both cases (1) and (2), the following pyrolysis law is imposed, to obtain closure:

$$m(T_s) = A_s e^{-\beta_s / T_s} \qquad (29)$$

One may proceed now to compare the present derivation and the BDP model, for AP and HMX; the appropriate input data are given in Tables 1 and 2. Experimental burning rate data for HMX and AP are taken from Price, Boggs and Derr [33], and for AP also from Hightower [34].

<div align="center">

TABLE 1

AP INPUT DATA
</div>

PROPERTY	UNITS#	PRESENT MODEL	BDP MODEL, PRESENT CALCULATION
λ_c	cal/cm-s-K	9×10^{-4} (c)	–
C_c	cal/g-K	0.5 (b)	0.3
ρ_c	g/cc	1.94 (a)	–
A_c	1/s	2.39×10^{18} (c)	–
E_c	kcal/mol	58.22 (c)	–
n_c	–	0 (c)	–
A_s	kg/m^2-s	1.29×10^7 (d)	3×10^6
E_s	kcal/mol	24.24 (d)	22
λ_g/C_p	kg/m-s	5×10^{-5} (e)	10^{-3}
C_p	cal/g-K	0.3 (c)	$0.3 = C_c$
$Q_c^* = Q_l^* + Q_{sub}^*$	cal/g	+444.6 (d)	$Q_f^* = +210$
Q_{sub}^*	cal/g	-591.5 (c)	$Q_s^* = +120$
K_l	$(kg/m^2\text{-s})^2/Pa^{n_l}$	$K_l = 1.387 \times 10^{-4}$ (g)	$K_l^0 = 9.619 \times 10^{-11}$ (g)
n_l	–	1.8 (f)	1.8
E_l	kcal/mol	42 (f)	30.
T_f	K	$1982 - 0.67 T_s$ (d)	1400
T_s-RANGE*	K	835-910 (c)	845-935

\# All actual calculations were performed using the SI system.

NOTES: (a) AMCP 706-177 Eng. Design Handbook [35]
       (b) Price, Boggs and Derr [33]
       (c) Guirao and Williams [32], calculated values
       (d) See comments following Table 2
       (e) Taken approximately from calculated values for RDX [31]
       (f) Longwell and Wise [36]
       (g) See Appendix B for calculations
       (*) 2 MPa-10 MPa

The following comments pertain to particular values of parameters used in the present model for AP as shown in Table 1.

The values of A_s, E_s in the pyrolysis formula were calculated from

$$\ln \dot{r} = \ln(A_s/\rho_c) - \beta_s/T_s$$

using the following two data points (r, T_s):

p(MPa)	r(cm/s)*	Ts(K)**
2	0.3	835
10	1.0	910

* Price, Boggs and Derr [33], r vs p (measured)
** Guirao and Williams [32], T_s vs p (calculated)

Thus, E_s = 24.24 kcal/mol, and A_s = 1.29 x 10^6 g/cm^2-s are obtained, using a sample density of 1.94 g/cc.

The value of Q_c^* = 444.6 cal/g was calculated from the global enthalpy balance,

$$C_c(T_s - T_o) + C_p(T_f - T_s) - Q_c^* = 0$$

with C_c = 0.5, C_p = 0.3, T_o = 300K, and T_s = 873K (at p = 4.5 MPa, reference point). Using this value of Q_c^*, one may obtain the linear dependence for $T_f(T_s)$ shown in Table 1. It should be noted that the "surface heat release" according to Eq. (12) is thus

$$Q_s^* = (1-G)Q_c^* + G\, Q_{sub}^* = 133.7 \text{ cal/g}$$

using Q_{sub}^* = -591.5 cal/g (from Guirao and Williams [32]) and G = 0.3. This value of Q_s^* is quite close to that inferred by BDP, namely, 120 cal/g.

18

TABLE 2

HMX INPUT DATA

PROPERTY	UNITS#	PRESENT MODEL	BDP MODEL PRESENT CALCULATION
λ_c	cal/cm-s-K	7×10^{-4} (a)	–
C_c	cal/g-K	0.43 (a)	0.3
ρ_c	g/cc (pressed pellets)	1.88	–
A_c	1/s	$10^{19.7}$ (b)	–
E_c	kcal/mol	52.7 (b)	–
n_c	–	1 (b)	–
A_s	kg/m^2-s	2.09×10^7 (c)	5×10^{10}
E_s	kcal/mol	19.59 (c)	50.
λ_g/C_p	kg/m-s	5×10^{-5} (c)	10^{-3}
C_p	cal/g-K	$0.43 = C_c$ (c)	$0.3 = C_c$
Q_{sub}^*	cal/g	-141.6 (f)	$Q_s^* = +225$
Q_l^*	cal/g	+453 (e)	$Q_f^* = +667.5$
T_f	K	1353 (e) (g)	3275
T_s-RANGE*	K	650-767	1085-1235
E_l	kcal/mol	46.2 (d)	$50 = E_s$
K_l^o	$(kg/m^2\text{-}s)^2/Pa^{n_l}$	1.017×10^{-7} (h)	4.34×10^{-12} (h)
n_l	–	1.4 (h)	2

\#   Actual calculations were performed using the SI system.

NOTES: (a)   AMCP 706-177 Eng. Design Handbook [35]
              (b)   Robertson [37]
              (c)   Ben-Reuven and Caveny [38]
              (d)   Shaw and Walker [39]
              (e)   Ben-Reuven [31]
              (f)   Rosen and Dickinson [40]
              (g)   This is only the nearfield-end temperature, not the
                     final flame temperature (3100 K at 20 atm).
              (h)   See calculations in Appendix B
              (*)   1 MPa-25.4 MPa

1.3   Discussion of Monopropellant Simulation Results

The formulation developed herein was used along with the BDP model to obtain parallel simulation of burning rate and pressure sensitivity data for both AP and HMX.

The results of burning rate vs pressure are shown in Fig. 5. The experimental data were taken from several sources [33,34] most of which were unavailable at the time the BDP model was developed. For this reason, both models were adjusted (single parameter fitted, pertaining to the chemical kinetics constant) at a single experimental reference point (p, m), as explained in Appendix B. The plots in Fig. 5 demonstrate that both models simulate well the AP burning rate, while the present model is clearly better for HMX in the pressure range below 10 MPa (100 atm).

The same HMX data set was previously used to obtain the parameters (c, B) in the following burning rate correlation,

$$ r = c \cdot p \cdot \left(1 + B/p \right)^{1/2} \tag{30} $$

derived in Ref. 38, and reproduced in Fig. 6. Evidently, simulation by Eq. (30) is superior to both BDP and the present model. This is not surprising, since Eq. (30) incorporates physical details pertinent to the complex nature of nitramine deflagration (namely, the concept of near-field and far-field, each dominated by a distinct chemical reaction mechanism). These details are completely missing from the BDP model, and were omitted from the present model (which is based entirely on the near-field) to facilitate the single delta-function flame approximation.

The pressure sensitivities due to each model are compared in Fig. 7, where the trends typical of AP (n decreasing with increasing p) and HMX (n increasing with increasing p) are demonstrated. Also shown is the remarkable capability of the BDP model to obtain both increasing and decreasing $n(p)$ with the same functional relationship, as mentioned earlier. The magic of this achievement is entirely due to the function $f_B(T_s)$, given in Eq. (26).

According to Eqs. (1) and (3), the BDP model provides $q = -\lg(z_B)$. From Eq. (3),

$$ T_s = (q + b_1)/b_0 \tag{31} $$

where $b_0 = C_c/Q_f^*$ and $b_1 = (C_c T_0 + Q_s^*)/Q_f^*$. Thus, Eq. (26) yields an expression in terms of q,

$$ \hat{f}_B(q) = \frac{(q + b_1)^2}{-q \ln q} \tag{32.a} $$

where the multiplicative constant $1/b_0^2$ has been omitted, without loss of generality. Note that b_1 is positive for net surface exothermicity, as assumed by BDP.[1] In general, $0 < q < 1$; at both ends of this domain, $f_B \rightarrow +\infty$, and the single extremal point, q^*, is defined by

$$\ell n\, q^* + (q^* + b_1)/(q^* - b_1) = 0 \qquad (32.b)$$

where $\hat{f}_B(q^*)$ is a minimum. Now, from the denominator of Eq. (25.a) one can readily see that whenever $\hat{f}_B$ increases, n will decrease, and vice versa for decreasing $\hat{f}_B$. Thus, the question of n(p) progressivity or regressivity in the BDP framework amounts to proper choice of parameters. The actual parametric ranges employed by BDP are as follows.

For AP, the range is

T_s (K)	p (MPa)	q	$\hat{f}_B$	z_B
830	1.58	0.186	4.50	1.68
970	18.4	0.386	5.23	0.95

for $b_0 = 1.43 \times 10^{-3}$ 1/K and $b_1 = 1.0$; $q^*(b_1) = 0.2137$ and $T_s^*(q^*) = 849K$, while $p^* = 2.34$ MPa. At this point n(p*) is maximal; thus, n will increase for $p < p^*$ and decrease for $p > p^*$, as shown in Fig. 7. This behavior is entirely extraneous to the physics built into the BDP model, and is not collaborated by experimental observation.

For HMX, the range is

T_s (K)	p (MPa)	q	f_B	z_B
1070	0.7	9×10^{-3}	5.46	4.71
1235	21.6	8.3×10^{-2}	1.49	2.49

for $b_0 = 4.49 \times 10^{-4}$ 1/K and $b_1 = 0.472$; $q^*(b_1) = 0.1478$, an order of magnitude higher than the HMX q-range. Thus, $T_s^*(q^*) = 1379$ K, and n(p) will be progressive throughout the range of p considered, as shown in Fig. 7.

Obviously, f_B variation for AP is moderate in comparison with that of HMX, since for AP the q-region straddles the f_B-min point. For HMX, the q-region is assigned (by proper choice of the T_s range and other parameters) away from the f_B-min point, so that f_B variation is more pronounced. Consequently, one may expect the BDP model to obtain steeper $n(p)$ and $\delta_p(p)$ variation for HMX than for Ap in the same pressure range. This is demonstrated in Figs. 7-11.

Regarding temperature sensitivity, both the BDP model and the present model seem to perform rather poorly when compared to the experimental data of Price, Boggs and Derr [33]. The associated data reduction for AP and HMX is shown in Figs. 8 and 9, respectively. Calculated and experimental values of δ_p vs p are depicted in Figs. 10 and 11. For AP, Figs. 8 and 10 demonstrate nonmonotonous behavior (with a minimum between 5 and 6 MPa), but relatively small overall variation: $100\ \delta_p$ between 0.2 and 0.3 1/K, for $1 < p < 10$ MPa. In the same pressure range, δ_p for HMX is monotonously decreasing, with a relatively large overall variation: $100\ \delta_p$ varies between +0.4 and -0.04 1/K, as shown in Figs. 9 and 11; crossing to negative values occurs roughly at 7 MPa. Note that the BDP results for HMX, although following the general trends at low pressures in Fig. 11, are still an order of magnitude too high.

The following conclusions can be drawn. Both the BDP model and the present model perform reasonably well in simulation of burning rate data, with a single parameter adjustment. Both models obtain explicit solutions, although the present model is somewhat more involved algebraically, on account of the input reactant fraction, $G(T_s,\ m;\ T_0)$, which is completely absent from the BDP formulation. Both models perform rather poorly in simulation of pressure- and temperature-sensitivity of burning rate.

The major difference between the models is quite apparent. The present model can be derived rationally from basic principles of combustion theory (using both energy and species conservation equations) and involves functional details (such as subsurface decomposition process and chemical kinetics data) specific to the monopropellant under consideration. In contrast, the BDP model incorporates an intuitive argument (extraneous introduction of chemical kinetics effects), while excluding specific physical details; consequently, the BDP formulation is not in agreement with known combustion theory, and characteristics of each monopropellant must be entered by proper choice of parameters and T_s-range. This parameter selection is often tenuous, as evident from the high values of T_s imposed for HMX (which seem more adequate for the outer end of the gaseous nearfield, where primary decomposition is complete), or from the n(AP)-max obtained inadvertently.

The delta-function approach developed herein is admittedly oversimplified (for HMX in particular), and seems too crude for anything but burning rate vs pressure simulation. It shows, nevertheless, that a reliable alternative to the BDP monopropellant model can be derived, and has potential for improvement, e.g., better subsurface decomposition formulation.

22

1.4   The BDP Composite Propellant Model

    This section addresses the problems associated with the BDP
combustion model, specifically pertaining to composite propellants,
as shown in the three parts of Fig. 3.

    The BDP model employs two consecutive flames in its physical
picture, cf Fig. 3.a, namely, the "monopropellant flame" and the
"final diffusion flame." Both are assumed adiabatic, and their
respective heat feedbacks to the surface are simply added; in other
words, the two flames are assumed independent of each other, or
decoupled. Obviously, conductive heat transfer from the external
(diffusion) flame must pass through the premixed monopropellant flame
region. An approximate double delta-function flame analysis (in which
the external flame position is assumed to be far downstream from the
inner flame) indicates that appreciable nonlinear coupling between
the external and inner flames should prevail. The following results
demonstrate this point.

    Suppose that the external flame has an exothermicity Q_2^*,
comparable to that of the inner flame, and is placed at a
dimensionless distance of z_2 from the surface, such that $z_2 \gg z_1$.
Thus, one may consider the external flame as a small perturbation
in the region close to the surface. The thermal enthalpy at the
position of the inner flame is

$$\theta_1 \equiv \theta(z_1) = \Lambda + C_2 e^{z_1 - z_2} - \left(\Lambda e^{-z_1} + C_2 e^{-z_2} \right) \quad (33)$$

where the last term in parantheses represents the dimensionless heat
feedback to the surface, and

$$C_2 \equiv \left(\frac{Q_2^*}{Q_1^*} \right) \frac{\lambda}{C_p} \Omega_2(p, T_2) / m^2 \quad (34)$$

Now, relative to the unperturbed, single delta-function inner flame,
the perturbation is

$$\delta\theta_1 = \theta_1 - \theta_1^o = C_2 e^{-z_2} \left(e^{+z_1} - 1 \right) \quad (35)$$

where $(\ )^0$ denotes unperturbed properties; note that $z_1 = z_1^0$ has been
assumed (as inferred from detailed calculations, cf Fig. 6 of Ref.
 38), as well as $\Lambda = \Lambda^o$. This leads to a perturbation of the inner
flame temperature, $T_1(z_1)$

$$\delta T_1 / T_1^o \sim \left(Q_1^* / C_p T_1^o \right) \delta\theta_1$$

23

and consequently, through the eigenvalue relationship in Eqs. (15), (16), the associated burning rate perturbation is

$$\delta m / m^0 \sim (\beta_1 / 2 T_1^0) \, \delta T_1 / T_1^0 \qquad (36)$$

with $(\beta_1 / 2 T_1) \sim O(10)$, demonstrating appreciable amplification. This nonlinear coupling effect is completely absent from the BDP composite propellant analysis, since adiabatic values of $T_1 = T_{fa}$ are specified, and the surface enthalpy balance (where all heat feedback components are linearly superimposed) is used to calculate the overall burning rate. It is therefore indicated that the BDP model is deficient in this respect of external/inner flame coupling, even if the physical model of Fig. 3.b is accepted.

Another puzzling aspect of the BDP composite model is that the parabolic (or conical) diffusion flame in the physical picture, cf Fig. 3, is transformed into a planar sheet parallel to the propellant surface in the physical model, Fig. 3.b. Then, in the analytical model, BDP assigns a value of $\exp(-c \cdot z_D)$ to the heat feedback due to this flame, where z_D is the dimensionless flame height, proportional to the actual height, X^*_{DF}, and c denotes a proportionality constant.

In an attempt to see whether such mean flame height is analytically plausible, an approximate calculation of the mean heat feedback is carried out, for a conical flame with a height of z_D. The configuration is shown in Fig. 12. The prevailing assumption is that the heat feedback contribution, due to each circular element of the conical flame surface, is proportional to $\exp(-z)$, where z denotes the element height. The contributions from the entire cone surface are then integrated, and the corresponding mean heat feedback to the oxidizer crystal surface is

$$\overline{q}_D \sim \frac{1}{\pi R_c^2} \int_0^{z_D} e^{-z} \, 2\pi (R_c - z \, tg\alpha) \, tg\alpha \cdot dz$$

$$= 2 (z_D - 1 + e^{-z_D}) / z_D^2 \qquad (37)$$

where R_c is the crystal radius. The expression obtained herein for the mean heat feedback, $\overline{q}_D(z_D)$, clearly precludes simple reduction to the form used by BDP, where z_D appears only as the exponential argument.

The final point to be raised in this conjunction concerns the validity of the so-called final diffusion flame. BDP postulated that this flame is diffusion controlled under all conditions, and without reference to particular chemical kinetics length or time scales. This means that chemical kinetics relaxation times are typically much shorter than diffusion times. Clearly, the reactant streams (emanating separately from binder pyrolysis and from oxidizer primary decomposition) are non-premixed or initially separate; further, the expected temperature range should be quite high, close to the adiabatic flame temperature of the oxidizer/binder configuration. All this seems to favor fast reaction kinetics and diffusion-controlled sheet flame. However, calculations carried out with chemical reaction length scales relevant to nitramine combustion demonstrate that some typical secondary reactions have length scales in the order of 100 microns and more. This is shown in Fig. 13; these scales are similar to typical hydrocarbon-oxidation reactions expected between binder chain fragments and oxidizer primary decomposition products for both AP and HMX. Moreover, oxidation reactions involving NO, a typical HMX decomposition product, are expected to be even slower. This strongly indicates that in some cases, specific to both propellant configuration and pressure regime, the final flame might be chemical-kinetics controlled, or that kinetics and diffusive processes might have comparable length and time scales.

1.5 Conclusions and Recommendations

The foregoing results point to several deficiencies in the BDP combustion model for composite propellants. These are: (1) The monopropellant (premixed) flame model does not agree with known combustion theory. (2) The analytical composite model combines linearly heat feedback from three different flame components without any consideration of thermal coupling, a prevalent nonlinear effect. (3) Heat feedback from the parabolical or conical flame surface is not adequately represented. (4) The final flame is assumed diffusion-controlled under all conditions, regardless of relevant chemical kinetics or pressure regime. Some of these defects could have been readily corrected. It can only be lamented that such a large amount of mental energy went, over a period of ten years, into considerations of granularity, modality, concave/convex particle surfaces, distinct vs uniform binder/oxidizer surface temperatures, etc., -- all in support of a semi-empirical correlation (exponential, not polynomial) which does not live up to its own physical model.

Evidently, this analysis indicates two main routes for future solid propellant combustion research. One, with an immediate engineering utility, would be to use directly Chebichev polynomials of the first kind to simulate burning rate vs pressure, with adjustable coefficients to account for granularity, modality, etc. These **must** work, since they involve exp(-z):

$$H_n(w) = \frac{(1-w^2)^{1/2}}{2(-i)^n} \int_{-\infty}^{+\infty} e^{-iwz} J_n(z) dz, \quad w < 1.$$
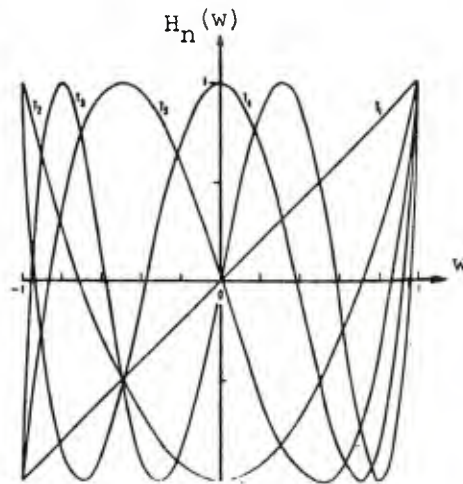
Chebichev polynomials, order n=1 through 5 plotted against normalized independent variable, w.

26

where J_n denote the associated Bessel functions of the first kind, and w is a normalized independent variable. These polynomials are routinely available in any respectable minicomputer software package, whereby a large number of coefficients can be adjusted with minimal effort.

The second way, by which physical insights might be obtained, would be through detailed analysis, using explicit chemical mechanisms and kinetics data in a comprehensive model, which may probably require numerical solutions of differential systems.

References

1. Beckstead, M.W., Derr, R.L. and Price, C.F., "The Combustion of Solid Monopropellants and Composite Propellants," _Proc. 13th Symposium (International) on Combustion_, The Combustion Institute, Pittsburgh, PA, 1970, pp. 1047-1056.

2. Beckstead, M.W., Derr, R.L. and Price, C.F., "A Model of Composite Solid Propellant Combustion Based on Multiple Flames," AIAA Jour. Vol. 8, No. 12, Dec. 1970, pp. 2200-2207.

3. Summerfield, M., et al., "Burning Mechanism of Ammonium Perchlorate Propellants," _Solid Propellant Rocket Research_, Progress in Astronautics and Rocketry, Vol. 1, Academic Press, N.Y., 1960, pp. 141-182.

4. Sutherland, G.S., "The Mechanism of Combustion of AP Polyester Resin Composite Solid Propellant," Ph.D. Thesis, Princeton University, Dept. of Aerospace, 1956, pp. 34-44 and 142-154.

5. Steinz, J.A. and Summerfield, M., "Low Pressure Burning of Composite Solid Propellants," _Propellant Manufacture, Hazards and Testing_, Advances in Chemistry Series, Vol. 88, American Chemical Soc., Washington, D.C., 1969, pp. 244-295.

6. Steinz, J.A., et al., "The Burning Mechanism of AP-Based Composite Solid Propellants," Ph.D. Thesis, Princeton University, Dept. of Aerospace, 1969.

7. Shultz, R., Green, L. and Penner, S.S., "Studies of the Decomposition Mechanism, Erosive Burning, Sonance and Resonance for Solid Composite Propellants," _3rd AGARD Colloquium_, AGARD, Pergamon Press, N.Y., 1958, pp. 367-427.

8. Williams, F.A. and Penner, S.S., "Analytical and Experimental Studies of the Steady State Combustion Mechanism of Solid Propellants," _Advances in Tactical Rocket Propulsion_, AGARD, 1967, pp. 131-134.

9. Beckstead, M.W. and McCarty, K.P., "Calculated Combustion Characteristics of Nitramine Monopropellants," _13th JANNAF Combustion Mtg._, CPIA Publication 281, Vol. 1, 1976, pp. 57-68.

10. Beckstead, M.W., "A Model for Solid Propellant Combustion," _14th JANNAF Combustion Mtg._, CPIA Publication 292, Vol. I, 1977, pp. 281-306.

11. Beckstead, M.W., "Modeling Calculations for HMX Composite Propellants," AIAA Paper 80-1167, AIAA Propulsion Conference, June 1980.

12. Beckstead, M.W., "Model for Double Base Propellant Combustion," AIAA Jour. Vol. 18, No.8, Aug. 1980, pp. 980-985.

13. Beckstead, M.W., "A Model for Composite Modified Double Base Propellants," AIAA Paper No. 82-0355, AIAA 20th Aerospace Sciences Conference, Orlando, Florida, Jan. 1982.

14. Cohen, N.S. and Price, C.F., "Combustion of Nitramine Propellants," 12th JANNAF Combustion Mtg., CPIA Publication 273, Vol. I, 1975, pp. 49-58. Also, Jour. of Spacecraft, Vol. 12, No. 10, Oct. 1975, pp. 608-612.

15. Cohen, N.S. and Strand, L.D., "Nitramine Propellant Research," 13th JANNAF Combustion Mtg., CPIA Publication 281, Vol. 1, 1976, pp. 75-87.

16. Cohen, N.S., and Strand, L.D., "Nitramine Propellant Research," NASA Tech Memorandum 33-801, October, 1976.

17. Cohen, N.S., "Review of Composite Propellant Burn Rate Modeling," AIAA Jour. Vol. 18, No. 3, Mar. 1980, pp. 277-293.

18. King, M.K., "Model for Steady State Combustion of Unimodal Composite Solid Propellants," AIAA Paper 78-216, AIAA Aerospace Sciences Mtg., Jan. 1978.

19. King, M.K., "Composite Propellant Combustion Modeling," AIAA Paper 80-1124, AIAA Propulsion Conference, June 1980.

20. Glick, R.L. and Condon, J.A., "Statistical Analysis of Polydisperse, Heterogeneous Propellant Combustion: Steady State," Proc. 13th JANNAF Combustion Mtg. CPIA Publication No. 281, Vol. II, pp. 313-345.

21. Glick, R.L., "Distribution Functions for Statistical Analysis of Monodisperse Composite Solid Propellant Combustion,"TN, AIAA Jour., Vol. 14, No. 11, Nov. 1976, pp. 1631-1633.

22. Glick, R.L., "On Statistical Analysis of Composite Solid Propellant Combustion," AIAA Jour., Vol. 12, No. 3, Mar. 1974, pp. 384-385.

23. Glick, R.L., "Statistical Analysis of Non-Metallized Composite Solid Propellant Combustion," CPIA Publication 243, Vol. I, 1973, pp. 157-184.

24. Hermance, C.E., "A Model of Composite Propellant Combustion Including Surface Heterogeneity and Heat Generation," AIAA Jour., Vol. 4, No. 9, Sept. 1966, pp. 1629-1637.

25. Krier, H., T'ien, J.S., Sirignano, W.A. and Summerfield, M. (KTSS), "Nonsteady Burning Phenomena of Solid Propellants: Theory and Experiments," AIAA Jour., Vol. 6, No. 2, Feb. 1968, pp. 278-285.

26. Theodore von Karman, "Structure and Propagation of Laminar Flames," Proc. 6th Symposium (International) on Combustion, The Combustion Institute, Pittsburgh, PA, 1957, pp. 1-11.

27. Zeldovich, Ya. B., "Chain Reactions in Hot Flames - An
    Approximate Theory for Flame Velocity," International Chemical
    Engineering, Vol. 2, No. 2, Apr. 1962, pp. 227-235.

28. Jain, V.K. and Kumar, R.N., "Theory of Laminar Flame Propagation
    with Non-Normal Diffusion," Combustion and Flame, Vol. 23,
    June 1969, pp. 285-294.

29. Bush, V.B. and Fendell, F.E., "Asymptotic Analysis of Laminar
    Flame Propagation for General Lewis Numbers," Combustion Science
    and Technology, Vol. 1, 1970, pp. 421-428.

30. Joulin, G. and Clavin, P., "Asymptotic Analysis of a Premixed
    Laminar Flame Governed by a Two-Step Reaction," Combustion and
    Flame, Vol. 25, 1975, pp. 389-392.

31. Ben Reuven, M., "Nitramine Monopropellant Deflagration and
    Nonsteady Reacting Rocket Chamber Flows," Ph.D. Thesis,
    No. 1455-T, Princeton University, Dept. of Aerospace, 1980,
    pp. 29-54.

32. Guirao, C. and Williams, F.A., "A Model for Ammonium Perchlorate
    Deflagration Between 20 and 100 Atm," AIAA Jour., Vol. 9, No. 7,
    July 1971, pp. 1345-1356.

33. Price, C.F., Boggs, T.L. and Derr, R.L., "The Steady State
    Combustion Behavior of Ammonium Perchlorate and HMX," AIAA Paper
    No. 79-0164, 17th AIAA Aerospace Sciences Mtg., Jan. 1979.

34. Hightower, J.D. and Price, E.W., "Combustion of Ammonium
    Perchlorate," 11th Symposium (International) on Combustion,
    The Combustion Institute, Pittsburgh, PA, 1967, pp. 463-470.

35. Engineering Design Handbook, AMCP-706-177, Explosive Series,
    Headquarters, U.S. Army Material Command, Jan. 1971.

36. Longwell, J.P. and Weiss, M.A., "High Temperature Reaction
    Rates of Hydrocarbon Combustion," Industrial and Engineering
    Chemistry, Vol. 4, Aug. 1955, pp. 1634-1643.

37. Robertson, A.J.B., "The Thermal Decomposition of Explosives,
    Part II. Cyclotrimethylenetrinitramine and Cyclotetra-
    methylenetetranitramine," Trans. Faraday Society, No. 45,
    1949, pp. 85-93.

38. Ben-Reuven, M. and Caveny, L.H., "Nitramine Flame Chemistry
    and Deflagration Interpreted in Terms of a Flame Model," AIAA
    Jour., Vol. 19, No. 10, Oct. 1981, pp. 1276-1285.

39. Shaw, R. and Walker, F.E., "Estimated Kinetics and
    Thermochemistry of Some Initial Unimolecular Reactions in the
    Thermal Decomposition of 1, 3, 5, 7 Tetranitro-1, 3, 5, 7
    tetraazacyclooctane in the Gas Phase," The Journal of Physical
    Chemistry, Vol. 31, No. 25, 1977, pp. 2572-2576.

40. Rosen, J.M. and Dickinson, C., "Vapor Pressures and Heats of Sublimation of Some High Melting Organic Explosives," <u>Journal of Chemical and Engineering Data</u>, Vol. 14, No. 1, January 1969, pp. 120-124.
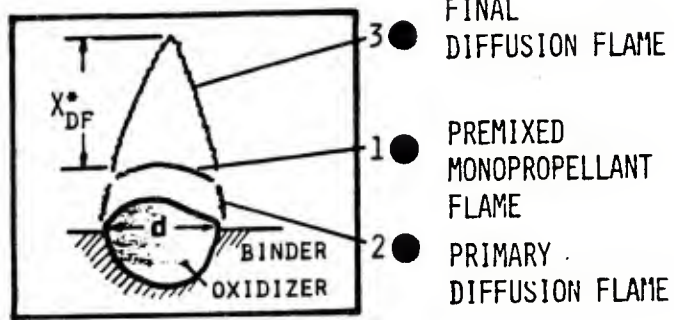
Fig. 1   The physical concept of burning composite
propellant, due to BDP.
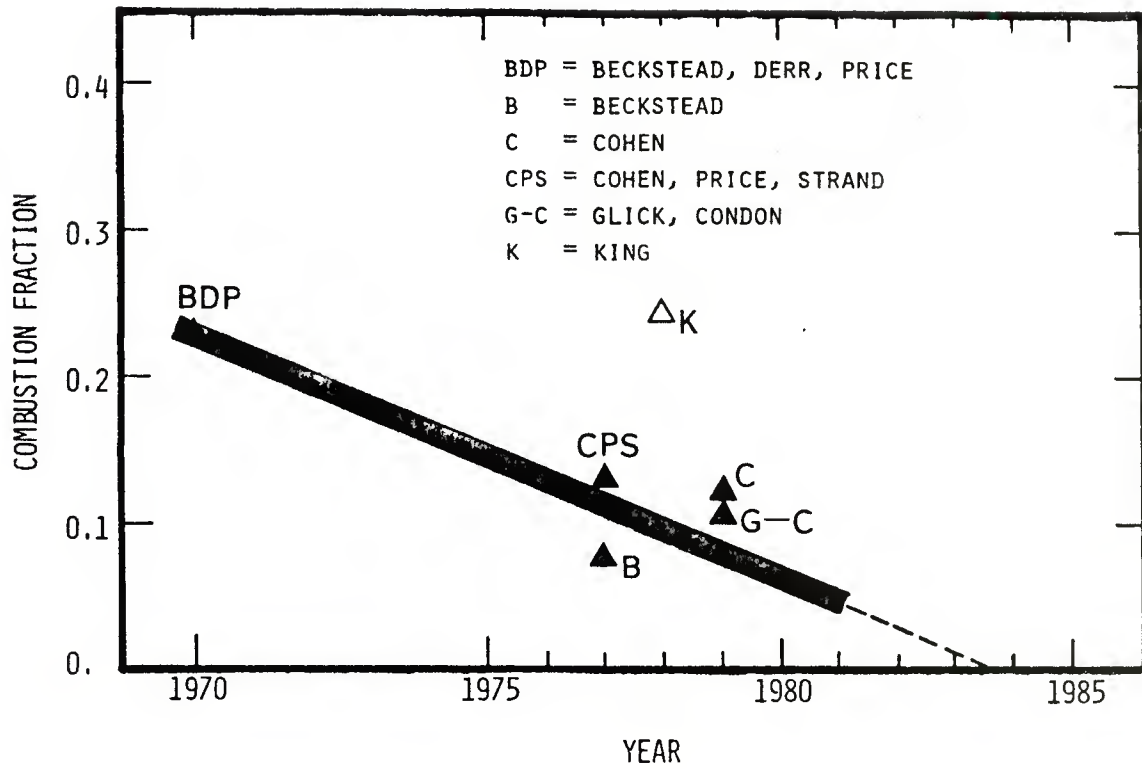
Fig. 2   The Combustion Fraction, an indicator of the relative importance
of combustion processes to various propellant burning models.   The
trend, obtained by least squares fit (excluding the model by King [18])
is obviously negative.
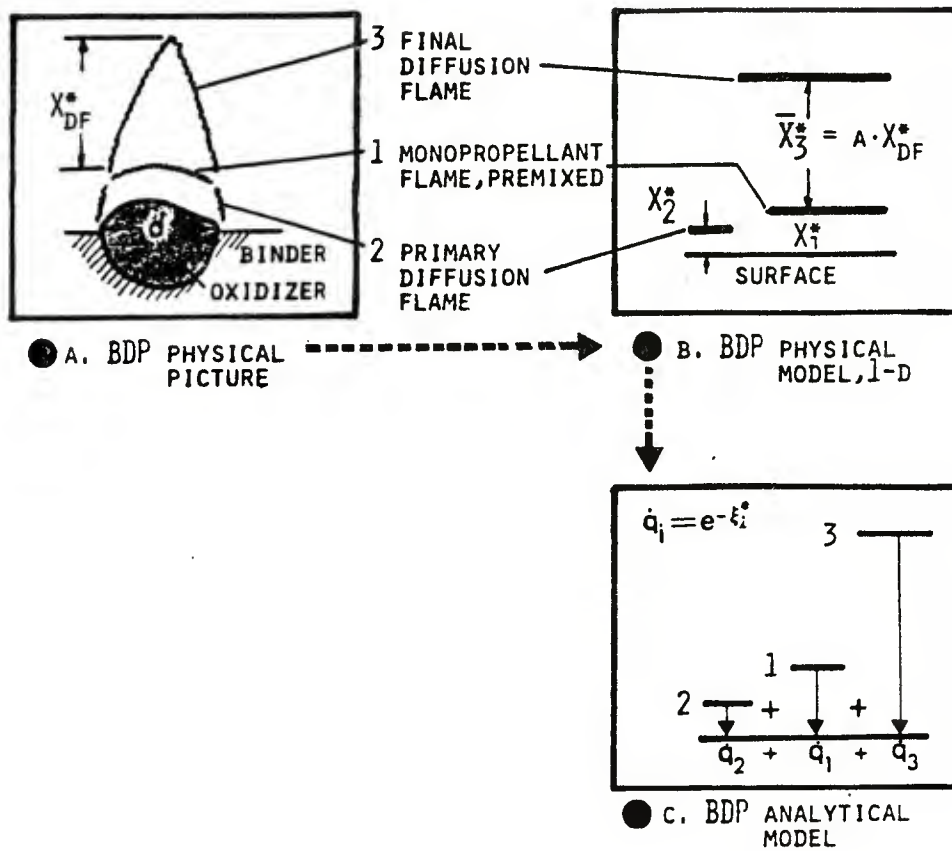
Fig. 3   Evolution of the BDP analytical model from the physical model
and the physical picture imposed by the authors.   One major question
in the critique herein is whether the three models are self-consistent.
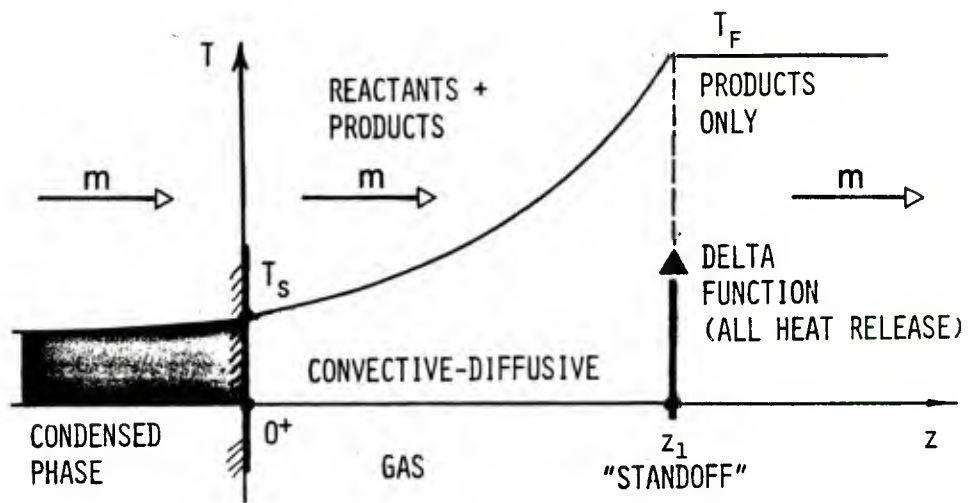
Fig. 4   The delta function approximation for the gas phase, used to
develop the present simplified model.   The delta function is imposed only
in the dimensionless physical coordinate system, $(\Theta, \mathcal{Z})$.
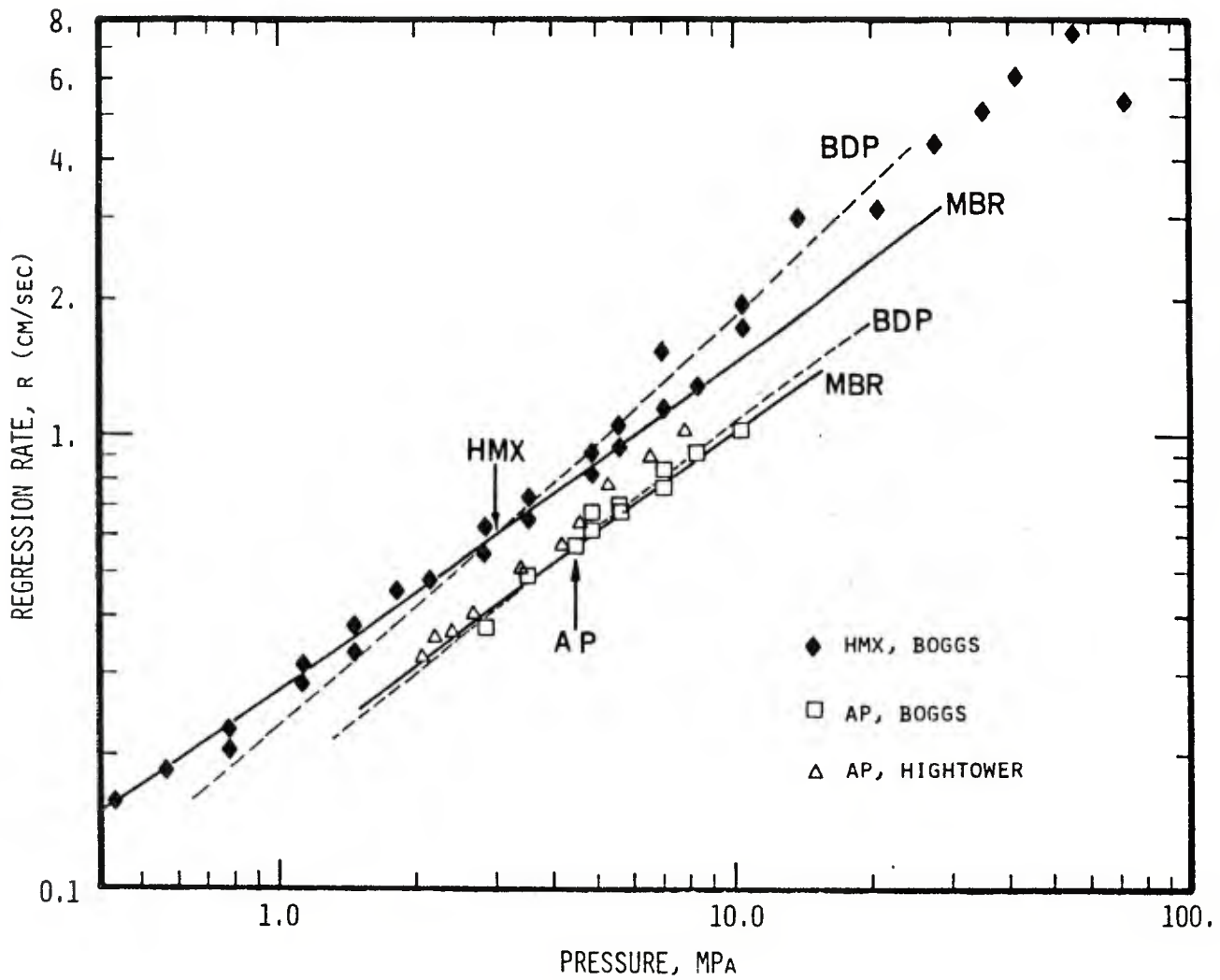
Fig. 5 Comparison of burning rate vs pressure for HMX and AP by both
BDP and the present model (denoted MBR), showing the latter to obtain
better correlation for HMX below 10 MPa.
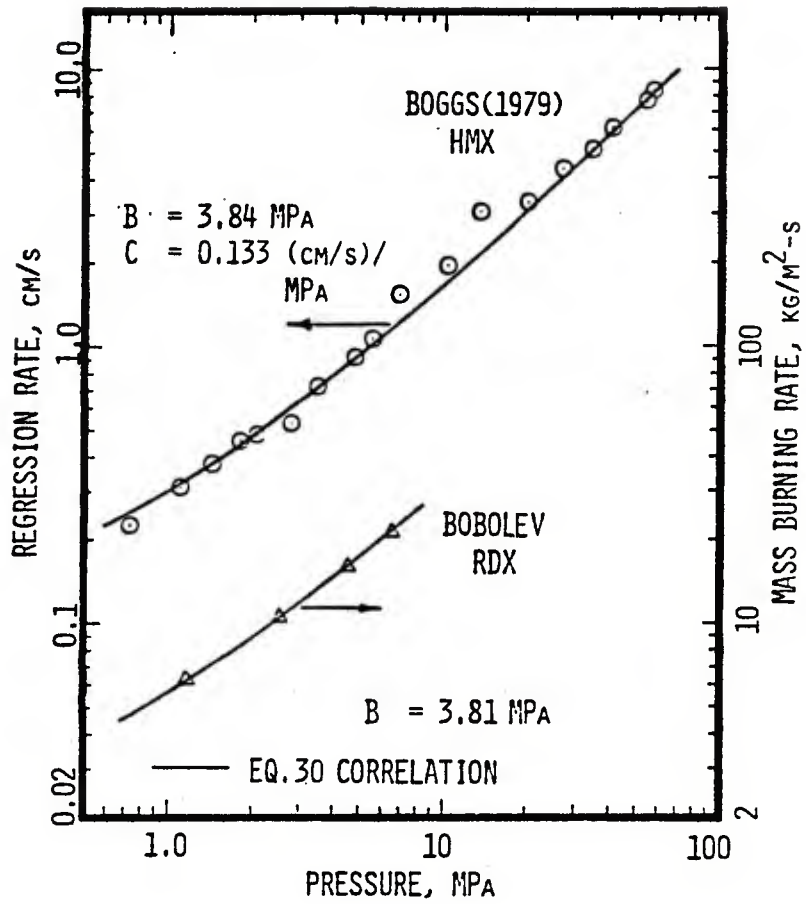
Fig. 6   Nitramine burning rate vs pressure - the same HMX data used in Fig. 5 is correlated by Eq. (30), demonstrating superiority over both BDP and the present model calculations.
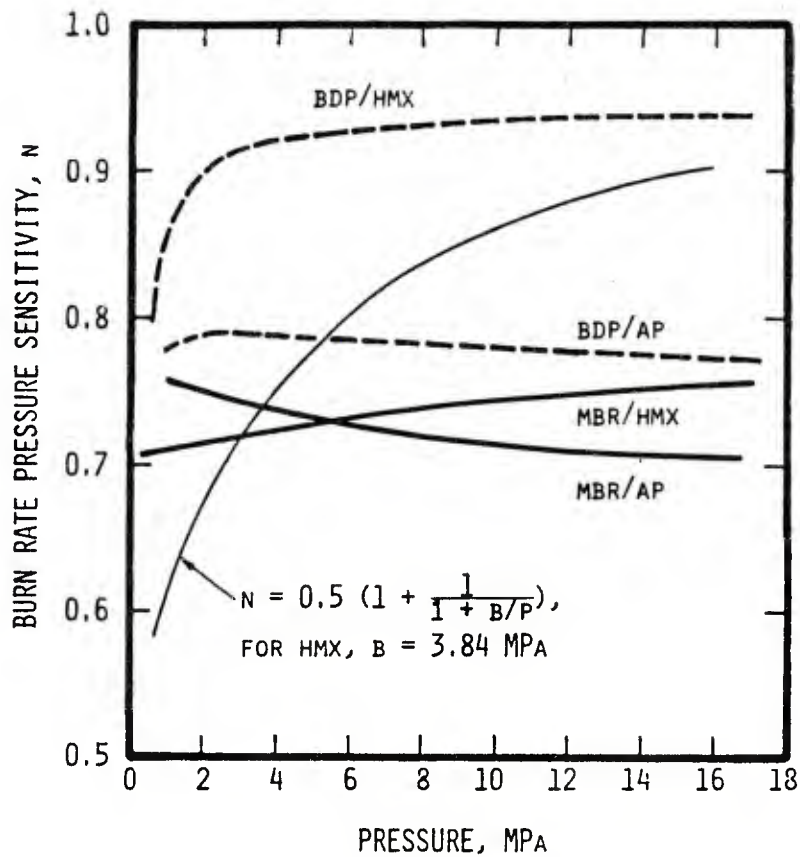
Fig. 7   Burning rate pressure sensitivity, η, calculated for both AP and HMX.   Both BDP and MBR models yield poor results for HMX, which is correlated by use of Eq. (30).
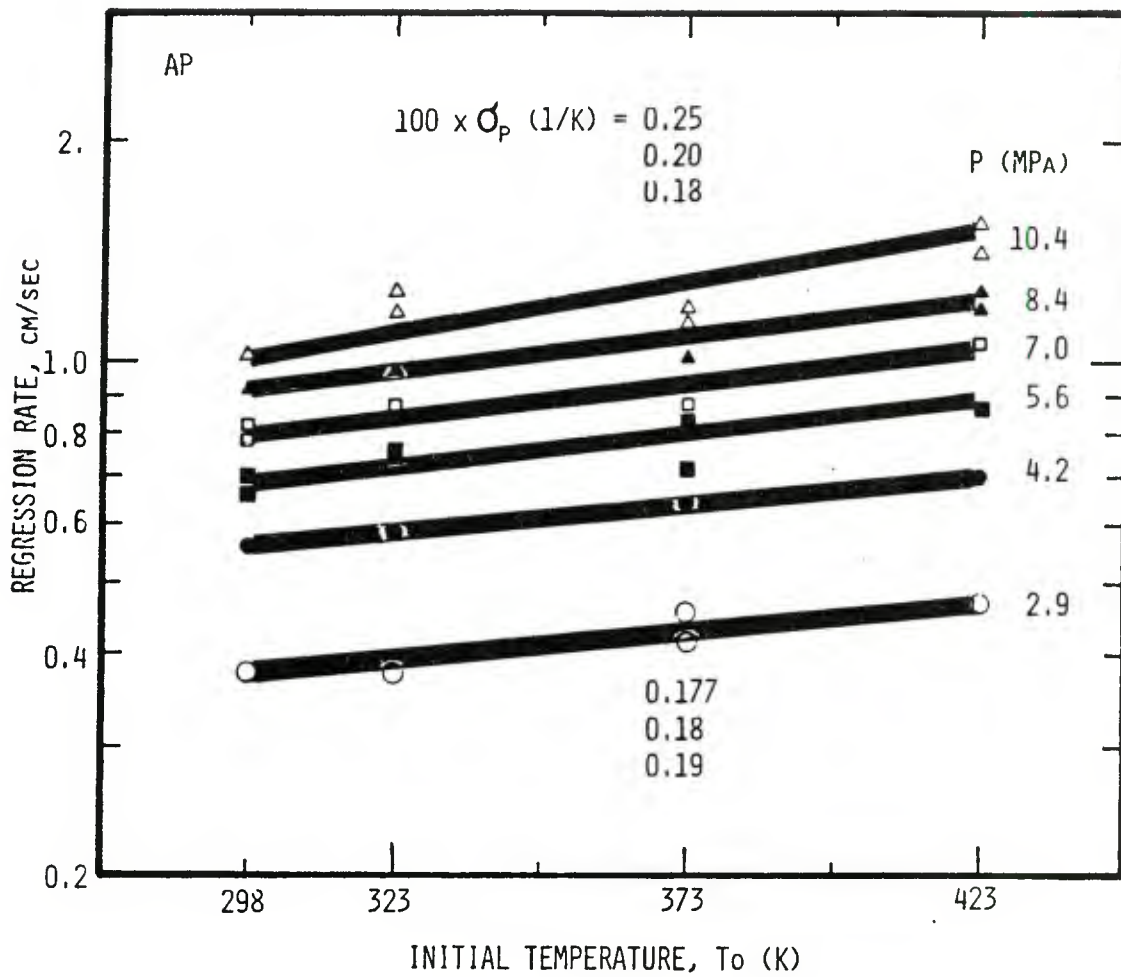
Fig. 8   Regression rate vs initial temperature for AP, with pressure as parameter.   Correlation of the experimental data by Price, Boggs et al [33].
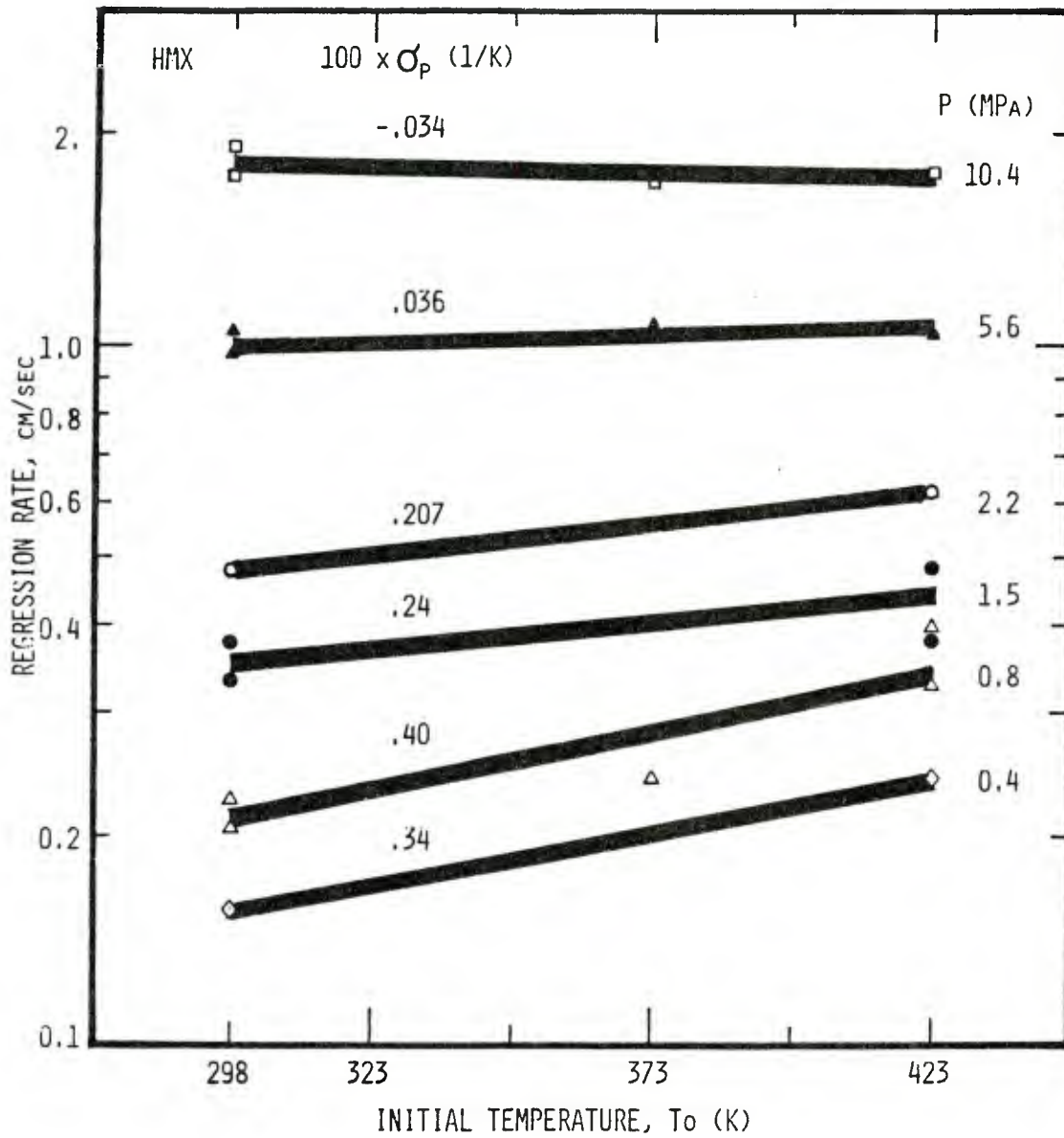
Fig. 9   Regression rate vs initial temperature for HMX, with pressure as parameter. Correlation of the experimental data by Price, Boggs et al [33].
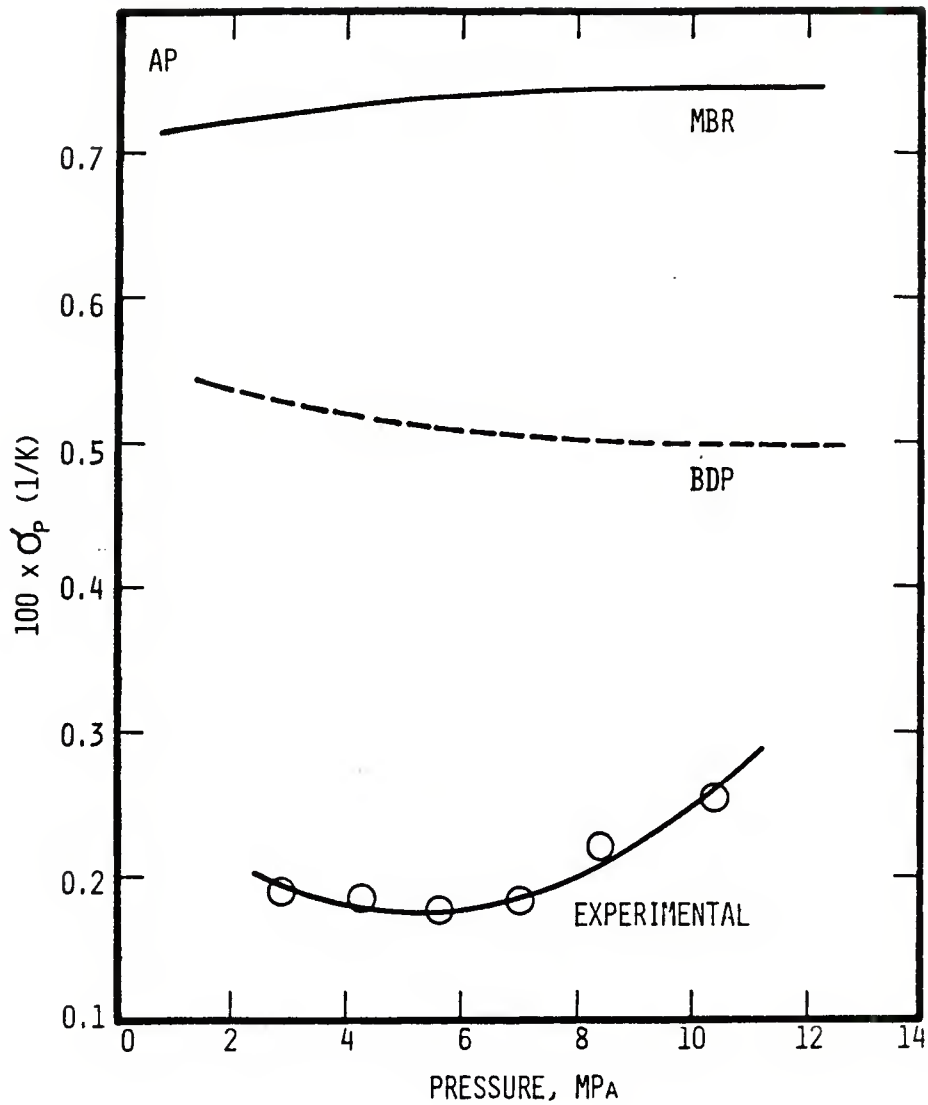
Fig. 10   Calculated and experimental temperature sensitivity vs pressure, for AP.   Experimental points are summarized from Fig. 8.
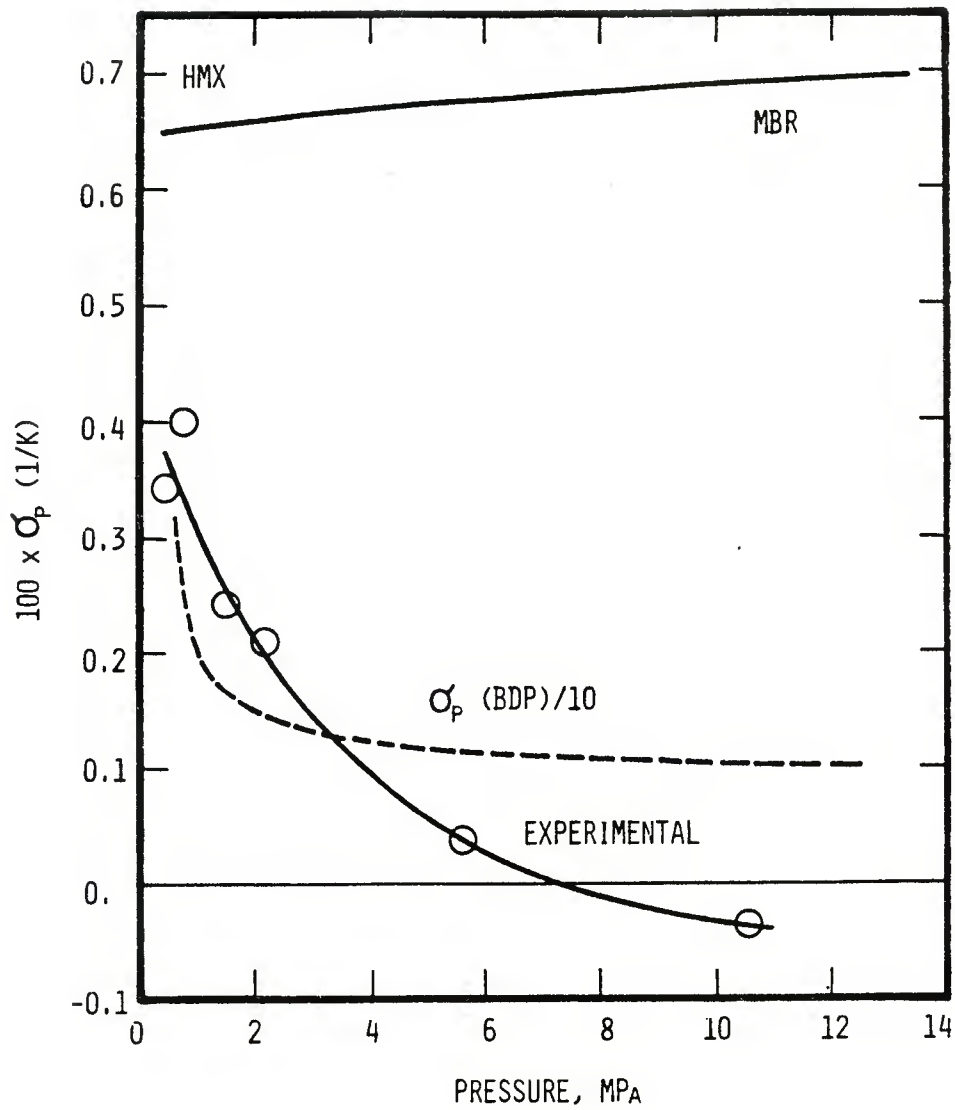
Fig. 11   Same as Fig. 10, for HMX.   The experimental trend is followed
by the BDP model to some extent, but an order of magnitude higher.
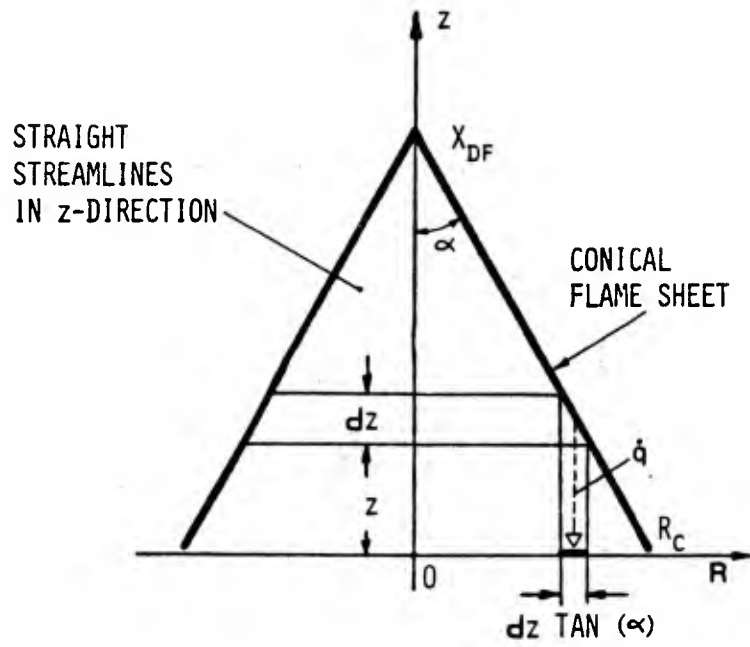
Fig. 12   The conical flame-sheet approximation, to calculate an integrated mean heat feedback to the surface.
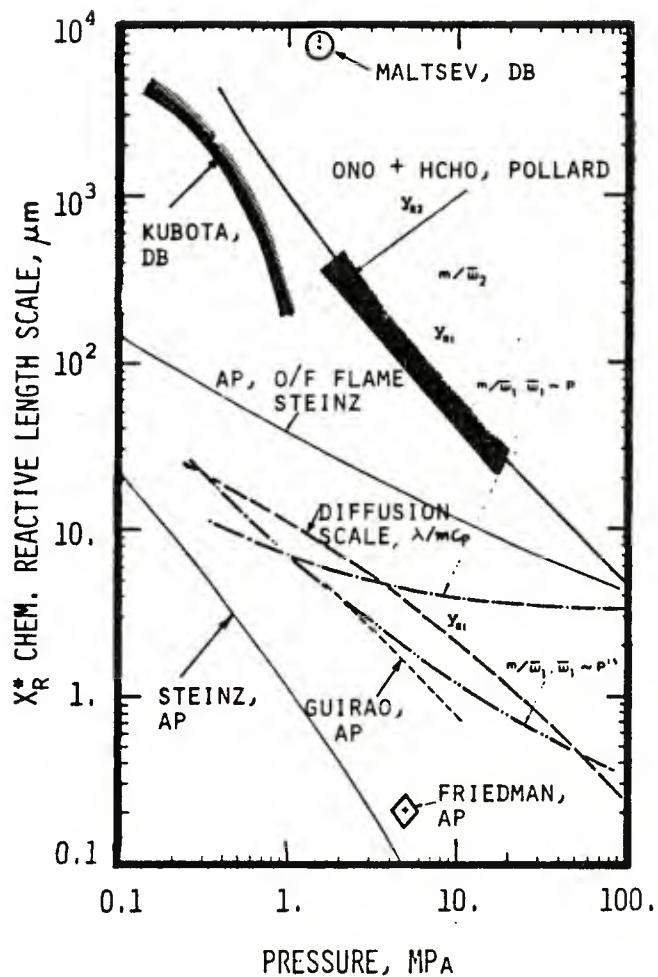
Fig. 13 Comparison of chemical reaction and diffusive length scales, relevant to AP and HMX. Even for the oxidizer (fuel flame of AP, calculated by Steinz [6]), the reactive and diffusive scales may be comparable, so the "final diffusion flame" concept of BDP should be re-examined.

44

II. A COMPREHENSIVE ANALYTICAL
MODEL FOR NITRAMINE DEFLAGRATION

1.1 Background

The foregoing section indicates that the complexity of nitramine monopropellant deflagration has not been considered in many composite propellant modeling efforts. Evidence to this complexity can be found in abundance in the nitramine chemical decomposition literature, a sample of which is given in Refs. 1-22; these works have been thoroughly reviewed in Ref. 23 and from the basis of a detailed analytical model [24, 25]; the present work is a direct extension of this model. Further reviews of published chemical analyses were performed by Schroeder [26-28].

The main objective of the present analysis is to enable burning rate prediction, i.e., calculation of m $(p;T_0)$ over a wide pressure range. Since the near-field in the gas phase has been treated in some detail previously [23-25], in terms of two global reactions, a natural extension would be to incorporate the entire gaseous flame (including the far-field) and to improve the melt phase model. This entails a larger number of secondary reactions and chemical species than previously considered. Further, in order to calculate the burning rate independently, full closure of the gas/melt interface conditions is required; this is provided by incorporation of a nonequilibruim evaporation law. This part of the study is motivated by the desire for better understanding of the nitramine combustion mechanism, and ways to affect changes in the burning rate, ultimately. The capability to compute the flame field structure (species and temperature profiles) as well as temperature and pressure sensitivities of the burning rate would enable comparison with experimental data for verification.

This leads, of course, to greater computational complexity and points up the relative lack of reliable chemical kinetics data. In this respect, the analytical model developed herein could serve to test various relevant chemical mechanisms and kinetics data, despite the higher degree of un-certainty involved.

The following sections describe the elements in the analysis which are new relative to Refs. 23-25: An extended (highly idealized) chemical mechansim for the gas phase, the melt phase model including decomposition gas bubbles, the gas phase model extended to include the far-field, and the nonequilibrium evaporation law.

1.2 CHEMICAL MECHANISM AND KINETICS

Nitramine deflagration probably involves two major sets of chemical reactions: (1) primary decomposition, first order overall, (in both condensed and gas phases) in which the molecular substance breaks up to form intermediate reactants, which is relatively fast and would occur close to the propellant surface, and (2) secondary reactions between the intermediate species, typically second order overall, relatively slow (compared with primary decomposition), by which the final composition and the final temperature evolve. This conceptual division into two rather diverse families of reactions is based on reported observations of the mechanism, products and kinetics of nitramine decomposition[1-22];it tends to be strongly supported by the measured shape of burning rate vs pressure curve, which exhibits a progressive pressure exponent n(p). For detailed discussions of the mechanism and kinetics of nitramine decomposition, the reader is referred to Refs. 23,24 and 25 .

The chemical reactions considered in the present analysis are as follows:

$$RDX(L) \rightarrow 3CH_2O + 9/4N_2O + 3/4NO + 3/8N_2, \quad Q=51.4 \text{ kcal} \quad (R.1)$$

$$RDX(G) \rightarrow NO_2 + N_2O + 3CH_2O + 3/2N_2, \quad Q=106.8 \text{ kcal} \quad (R.2)$$

$$5/7CH_2O + NO_2 \rightarrow NO + 3/7CO + 2/7CO_2 + 5/7H_2O, \quad Q=46 \text{ kcal} \quad (R.3)$$

$$CH_2O + N_2O \rightarrow H_2O + CO + N_2, \quad Q = 76.1 \text{ kcal} \quad (R.4)$$

$$CH_2O + NO \rightarrow H_2O + CO + 1/2N_2, \quad Q = 78.1 \text{ kcal} \quad (R.5)$$

$$CO + H_2O \rightarrow CO_2 + H_2, \quad Q = 9.9 \text{ kcal} \quad (R.6)$$

$$CO_2 + H_2 \rightarrow CO + H_2O, \quad Q = -9.9 \text{ kcal} \quad (R.7)$$
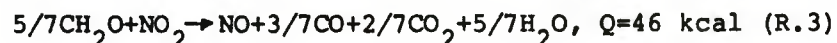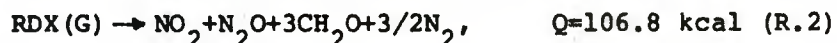
where $Q > 0$ denotes exothermicity. All the reactions (R.2) through (R.7) can occur simultaneously at any point in the gaseous flame field. The global mechanisms postulated for reactions (R.4) and (R.5) are purely conjectural, and merely intended to produce observed final products. The relevant chemical kinetics data is given in Table 1. It should be emphasized that the list of chemical reactions herein is in no way conclusive. Many more reactions may be relevant to the gas phase during nitramine deflagration; further, some intermediate products might have a strong influence upon the far-field structure, the final composition, and final temperature attained. The algorithm constructed in this study for solution of the conservation equations in the gas phase anticipates progress in the detailed knowledge of relevant mechanisms and chemical kinetics data. Incorporation of additional chemical reactions in the model involves merely

modifications of the input data set, as the reaction terms are handled in a completely generalized manner in the algorithm. For accomplishment of this flexibility, the list of chemical species (and the specific thermophysical data associated with them, such as specific heats, conductivities and viscosities, molecular weights, etc), is more extensive than would be required by the foregoing list of reactions, and is as follows:

nitramine (RDX or HMX), H_2O, CH_2O, CO_2, CO, N_2,

NO, N_2O, NO_2, HCN, HNO_2, H_2, H, HO, and $(-CH_2-)$

Evidently, reactions by which HCN + HONO, or HONO 4-center elimination occur were excluded from the present analysis. HONO-elimination was suggested by Shaw and Walker[20] as a possible initial step of nitramine decomposition, later followed by Schroeder, [26-28] and recently by McGuire and Traver[29]; all these works involve theories, not measurements. Experimentally, the Electron Spin Resonance (ESR) spectroscopy conducted by Beyer and Morgan[30] indicated the presence of HCHN and NO_2 during decomposition of RDX and HMX; these may lead to subsequent HCN + NO_2 reaction; however, HONO-elimination is not a necessary step and HCHO production is still present. It must be stressed that identification of large molecular fragments of 74 and 148 amu by Goshgarian[16] and by Farber and Srivastava,[31] by mass spectroscopy of decomposing RDX and HMX do not lend any evidence to the HONO-elimination schemes; rather, further support is obtained for the widely observed HCHO, NO_2 and N_2O decomposition products. For these reasons, the reactants HCN and HONO are incorporated in the data set of the present analysis, but the corresponding reactions were suspended until further experimental evidence points out their relevance. As to HCN oxidation by NO_2, the high-temperature and pressure (but dilute mixture) measurements by Fifer and Holmes[32] indicate that this overall reaction is slower by 1 to 3 orders of magnitude than the parallel NO_2 + HCHO reaction in the range 1000-1500k typical to the end of the gaseous near field in the deflagration process, which means that the HCN + NO_2 oxidation does not influence the heat feedback to the propellant surface appreciably.

1.3 ANALYSIS

Generally, the physical model of nitramine monopropellant deflagration herein is quite similar to the models discussed in detail by Ben-Reuven et al; [23-25] therefore, only those elements of the present analysis which are distinct will be presented. In particular, (1) incorporation of gas bubbles in the melt layer, (2) extension of the analysis to include the far-field in the gas phase, and (3) addition of a nonequilibrium nitramine evaporation law, to facilitate independent calculation of the mass burning rate, m.

The physical models for the gaseous deflagration wave and the melt layer are depicted in Figs. 1 and 2, respectively. The analytical method employed is to define and solve separately well-posed problems in each region (melt, and gas phase), and then match the solutions at the melt/gas interface by satisfying the available mass, species and energy conservation constraints.

1.4 CHEMICALLY REACTING MELT LAYER WITH GAS BUBBLES

The presence of gas bubbles in the melt layer of deflagrating neat nitramines (RDX and HMX) has been inferred from electron microscope photography of extinguished sample surfaces [33].Their relevance to the actual deflagration process was further indicated in a previous theoretical analysis[25],where the effect of bubbles was identified a posteriori by an approximation (which allowed a unique correlation between the imposed global heat of reaction in the layer and pressure). The melt layer analysis herein incorporates gas bubbles a priori, through a two-phase flow treatment.

It should be emphasized that even with 1% subsurface decomposition in which bubbles are formed, the local mean density would be appreciably lower than the neat liquid density; of course, this follows from the great diversity in intrinsic densities at moderate pressures: $\rho_C^* \gg \rho_G^*$. Similarly, since thermal conductivities are related approximately as $\lambda_c/\lambda_G \sim O(10)$, the porosity, due to the presence of bubbles, can effectively decrease the conductive heat transfer in the layer. In comparison, the available data show that $C_c \doteq C_p$ (gas) in the range of temperatures considered.

The following simplifying assumptions have been employed:
(1) Bubbles are small relative to the overall layer thickness.
(2) Bubbles are small enough such that thermal relaxation within the bubbles and between the bubbles and the liquid can be considered instantaneous, and a uniform local temperature, $T_c = T_G$ prevails at each point. (3) Mean intrinsic thermophysical properties (conductivities and specific heats) are uniform throughout the layer, as well as the liquid density, ρ_c^*. (4) Further, the pressure throughout the layer is uniform: $dp/dy = 0$, and equal to the external pressure prevailing in the gas phase domain. (5) Although thermal diffusion is incorporated, chemical species diffusion (due to concentration gradients) is assumed negligible in the layer; note, however, that the gas may percolate through the liquid, as a nonzero velocity-slip is permissible.

For two interpenetrating media, the total volume is $V = V_g + V_c$. The porosity or "void-fraction" is then $\Psi = V_g/V$, while the overall mixture density is defined

$$\rho_B = \left(\frac{\Psi}{\rho_c^*} + \frac{1-\Psi}{\rho_G^*} \right)^{-1} \qquad (1)$$

where $\rho_c^* \doteq const$, and $\rho_G^* = p \bar{W}_g/R_u T$ are the intrinsic liquid and gas densities, and Y denotes the overall liquid mass fraction. According to the foregoing definition of porosity,

$$\Psi = (1-Y)\rho_B/\rho_G^* \qquad (2)$$

48

Similarly,

$$1-\Psi = V_c/V = Y\rho_B/\rho_c^*$$

both of which will become useful later. The mass conservation
equations arise from a continuum derivation for two phase flow, such
as given by Nigmatulin [34]; at steady state,

$$\frac{d}{dy}\left[\Psi\rho_G^* u_G\right] = \frac{d}{dy}\left[(1-Y)\rho_B u_G\right] = \omega_c \quad (3a)$$

$$\frac{d}{dy}\left[(1-\Psi)\rho_c^* u_c\right] = \frac{d}{dy}\left[Y\rho_B u_c\right] = -\omega_c \quad (3b)$$

ω_c (kg/m^3-s) denotes the mass exchange rate between the phases, due
to liquid nitramine decomposition by which a gas mixture evolves,

$$\omega_c = A_L e^{-\beta_L/T(y)}(\rho_B Y) \quad (4)$$

Summation over the two mass conservation equations yields the overall
constraint: dm/dy = d/dy(m$_g$ + m$_c$) = 0, from which

$$(1-Y)\rho_B u_G + Y\rho_B u_c = m(y) = \rho_c^* r = const \quad (5)$$

determined at the solid/liquid boundary, where $Y(- y_m) = 1$, and
$u_c(- y_m) \doteq r$. The formal similarity between the foregoing
differential equations for liquid and gas can be utilized, so that
only one need be solved (e.g., the liquid phase), as will be shown
later.

The liquid phase momentum equation in the layer is

$$\frac{d}{dy}\left[(1-\Psi)\rho_c^* u_c^2\right] + (1-\Psi)\frac{dp}{dy} = -u_c\omega_c \quad (6)$$

which reduces to du$_c$/dy = 0, or

$$u_c(y) = r = const \quad (7)$$

where assumption (4) and Eq.(3.b) have been applied. No useful
information is obtained from the gas phase momentum equation, since
with u$_c \doteq$ r and $_G^*$ fully determined by T(y), one may obtain
algebraically from Eq. (5),

$$u_G(y) = m/\rho_G^*(T(y)) \quad (8)$$

which is similar to the definition of velocity in the gaseous flame
field, where m = const and p = const are likewise assumed.

Utilizing assumptions (2) and (3), the combined energy equation (over both gas and liquid phases) is written in terms of the overall thermal enthalpy, $h_c \doteq C_B (T - T_0)$:

$$m\frac{dh_c}{dy} + \frac{d}{dy}\left[-\frac{\lambda_B}{C_B}\frac{dh_c}{dy}\right] = Q_L^* \omega_c \qquad (9)$$

where $C_B \doteq C_c \doteq C_p$ = const, and

$$\lambda_B \doteq \psi\lambda_G + (1-\psi)\lambda_c \qquad (10)$$

the overall conductivity is now obviously variable through the layer, through its dependence upon the porosity. It should be emphasized that the layer thickness is not known beforehand; however, three boundary conditions are available for the energy equation, viz.,

$$T(-y_m) = T_m, \qquad T(0) = T_s$$

$$\lambda_B \frac{dT}{dy}(-y_m^+) = m\left[C_c(T_m-T_0) + Q_m^*\right]. \qquad (11)$$

which help overcome this difficulty. The following coordinate transform is used:

$$z \equiv \int_{-y_m}^{y} \frac{dy'}{\lambda_B/mC_B} \qquad (12)$$

This transform, and the dimensionless variables $\tau \equiv (T-T_m)/(T_s-T_m)$, and $X \equiv \varrho_B Y/\varrho_c^*$ reduce the differential system for $0 < z < z_s$ to:

$$\frac{d}{dz}\left(\tau - \frac{d\tau}{dz}\right) = \widetilde{Q}_c \widetilde{\omega}_c \qquad (13)$$

$$\frac{dX}{dz} = -\widetilde{\omega}_c \qquad (14)$$

$$\tau(0)=0, \quad d\tau/dz(0)=\left[Q_m^* + C_c(T_m-T_0)\right]/C_c(T_s-T_0),$$
$$X(0) = 1. \qquad (15)$$

where $\widetilde{Q}_c \equiv Q^*/C_c(T_s-T_m)$, $\widetilde{\omega}_c \equiv (\lambda_B/C_B m^2)\omega_c$ and z_s defined by Eq. (12), with upper limit of 0. A final transform to τ as independent variable, with $\phi \equiv \tau - d\tau/dz$ and z as dependent variables, obtains, for $0 < \tau < 1$:

$$d\phi/d\tau = \widetilde{Q}_c \widetilde{\omega}_c/(\tau-\phi) \qquad (16)$$

$$dz/d\tau = 1/(\tau-\phi) \qquad (17)$$

$$\phi(0) = -d\tau/dz(0), \qquad z(0) = 0. \qquad (18)$$

50

while $X(\tau)$ is given at each point by the coupling coefficient

$$C_X \equiv \phi(\tau)/\tilde{Q}_c + X(\tau) = \frac{1}{\tilde{Q}_c} \frac{d\tau}{dz}(0) + 1 = const. \quad (19)$$

where the self-similarity between ϕ and X in Eqs. (13) and (14) has been exploited. Of course, an additional integration is necessary to determine y from the dimensionless z.

The formulation in this section therefore obtains a closure, by which all of the layer properties of interest (including Y, dT/dy, ρ_B, u_g and ψ) can be caluclated as functions of temperature, with (m, T_s; $\hat{p}$, T_0) as parameters. The major physical difference between the present melt layer model (with bubbles) and the previous ones [23,25] ,(without bubbles) is that pressure effects are incorporated explicitly herein, whereas in the previous models solutions could be generated for specified (m, T_s; T_0) data.

The differential system of Eqs. (16) through (18) was integrated numerically, using a Runge-Kutta-4 method.

1.5 THE GAS PHASE REGION, INCLUDING THE FAR-FIELD

In the case of nitramine deflagration at moderate pressures, the diversity of chemical kinetics length scales (between rapid primary decomposition and much slower secondary reactions) implies that the gas phase region is divided into two distinct parts: the near-field, adjacent to the surface, where rapid change and high gradients occur, and the far-field, where changes in composition and temperature are much more moderate in comparison.

Employing standard assumptions (for a discussion, see Refs. 35 and 23), the dimensionless conservation equations for chemical species mass fractions and thermal enthalpy are, in the region $0 < \zeta < \infty$:

$$dY/d\zeta - d^2Y/d\zeta^2 = \frac{\rho D}{m^2} \sum_{i=1}^{M} W_j \Delta v_j^{(i)} \omega_i , \qquad (20)$$

$$j = 1, 2 \cdots N$$

$$dh/d\zeta - d^2h/d\zeta^2 = \frac{\lambda/C_p}{m^2} \sum_{i=1}^{M} \widetilde{Q}_i^* \omega_i \cdot \qquad (21)$$

where ω_i (mol/m^3-s) denote overall reaction rates, and the diffusivities are $\lambda/C_p \doteq \rho D$, equal for all species, but allowed to vary with both local composition and temperature. The dimensionless coordinate ζ and the thermal enthalpy are, respectively,

$$\zeta \equiv \int_0^{y} \frac{dy'}{\lambda/mC_p} \qquad (22)$$

$$h \equiv \frac{1}{Q_\lambda^*} \int_{T^o}^{T} C_p(T')dT' \qquad (23)$$

where T^o is the standard reference temperature and Q_1^* denotes the heat of primery nitramine decomposition in the gas phase (J/kg). Note that $m(\zeta) = $ const. The boundary data specified are:

$$Y_j(0^+) = Y_j^o , \quad h(0^+) = h(T_s, Y_1^o, \cdots Y_N^o) \qquad (24a)$$

$$Y_j(\infty) = Y_{jf} , \quad T(\infty) = T_f , \quad dY_j/d\zeta(\infty) = dh/d\zeta(\infty) = 0. \qquad (24b)$$

Since, as mentioned earlier, the gaseous flame field involves diverse length scales, the following transform was used, for practical purposes:

$$\eta \equiv \ln(\zeta + c) \qquad (25)$$

with c > 0 being an adjustable constant, which allows controlled streching of the near-field coordinate, while compressing the far-field length scale. It also affords sufficient spatial resolution in the far-field (e.g., for specified ζ_{max} = 1000 and c = 0.3, η_{max} = 6.91 and η_{min} = -1.2).

Using the foregoing transform, the gas phase conservation equations can be expressed as

$$(1+e^{\eta})\frac{d\phi}{d\eta} - \frac{d^2\phi}{d\eta^2} = e^{2\eta}\widetilde{R}(\phi), \quad \eta_{min} \leq \eta < \eta_{max}$$

(26)

where $\phi(\eta)$ represents dimensionless gas phase variables (species mass fractions thermal enthalpy) and R denotes the sum of relevant chemical reaction terms, as in Eqs. (20), (21). For $\eta \leq 0$ (the near-field), the formulation gives approximately

$$d\phi/d\eta - d^2\phi/d\eta^2 \doteq \varepsilon\widetilde{R}(\phi)$$

(27)

where $0 < \varepsilon \leq 1$ (but where reaction terms are relatively large), while for $\eta > 0$ (the far-field), the diffusion term is relatively suppressed, and a convective-reactive flow prevails:

$$d\Phi/d\eta \doteq e^{\eta}\widetilde{R}(\Phi)$$

(28)

Note that for large values of η, the chemical reaction rates are expected to be vanishingly small, compatible with the boundedness constraint imposed in Eq. (24.b). Independent solution manifolds can now be generated for the gas phase conservation equations (transformed)[25], for specified data (m,p) and $\phi(\eta_{min}) = \phi^o$. The latter data, of course, are not known a priori. Therefore, the relevant interface conservation conditions at the melt/gas interface must be satisfied to render the overall solution (carried out separately for the melt layer and the gas phase) physically meaningful. For chemical species and thermal enthalpy, following Scala and Sutton [36],

$$\phi(0^+) - d\phi/d\zeta(0^+) = \phi(0^-)$$

(29)

where, for chemical species

$$\phi(0^-) = Y_j(0^-), \quad j = 1, 2 \cdots N$$

(30)

and for thermal enthalpy,

$$\phi(0^-) \equiv \left[mC_B(T_s - T^o) - \lambda_B\frac{dT}{dy}(0^-) \right.$$

$$\left. - mY_R(0^-)Q_v^* \right] / mQ_1^*$$

(31)

53

where the right-hand sides and the left-hand sides of Eqs. (29) are fully determined by the melt layer and the gas phase solutions, respectively. Those solution manifolds which satisfy the interface conservation conditions, Eqs. (29)-(31), are physically genuine solutions pertaining to the particular (m, p, T_0) data set imposed.

1.6   THE NONEQUILIBRIUM NITRAMINE EVAPORATION LAW

To facilitate independent calculation of the burning rate, m, with the present model, an additional physical constraint is required. This physical condition is provided by the nonequilibrium evaporation law at the melt/gas interface.

The process of evaporation, at any instant, involves molecules of the substance (R) leaving the liquid in an outward flux, m_R(out), and an influx of molecules effectively returning to the surface, m_R(in). When the net effect is m_R(out) = m_R(in), the vaporization is termed at   equilibrium. However, when m_R(out) $\neq$ m_R(in), net evaporation takes place, as it is assumed to occur at the surface of deflagrating nitramines. In this instance, the net vaporizing material flux can be expressed [37] as,

$$m_R = \alpha_k \rho_s U_{ms} \left[Y_R^{eq}(0^+) - Y_R(0^+) \right] \qquad (32)$$

where $0 < \alpha_k < 1$ denotes the Knudsen accomodation coefficient, ρs is the gas density at the surface; the mean __molecular__ velocity perpendicular to the surface is

$$U_{ms} \doteq \left(R_u T_s / 2\pi W_R \right)^{1/2} \qquad (33)$$

and Y_R^{eq} and Y_R denote the equilibrium- and actual-mass fractions of 'R' on the gas side of the surface, respectively. The outward flux, m_R(out) is always given by the equilibrium expression,

$$Y_R^{eq}(0^+) = \left[p_R^{eq} / P \right] W_R / \overline{W}_s \qquad (34)$$

$\overline{W}_s$ is the mean molecular weight of gas at the surface, and p_R is the partial pressure of 'R', where use have been made of Dalton's law. Using a Clansius-Clapeyron expression,

$$p_R^{eq} = P_v \exp\left[\int_{T_v}^{T_s} \frac{Q_v dT}{R_u T^2} \right] \qquad (35)$$

with P_v and T_v being the measured low temperature reference values.

The net vaporizing flux, therefore, is the difference between two large numbers, since $U_{ms} \gg U_{gs}$. Thus, Y_R^{eq} and Y_R (actual) must

55

be comparable to obtain the moderate values of m observed; indeed, $Y_R^{eq}(0^+)$ is expected to yield a good estimate of the actual value of $Y_R(0^+)$, but their difference becomes important whenever m is to be calculated.

Note that the total mass flux in the present system is

$$m = m_R + m\left[1 - Y_R(0^-)\right]$$

accounting for subsurface decomposition in the melt layer; hence,

$$m = m_R / Y_R(0^-) \qquad (36)$$

which serves, along with the foregoing formulation leading to m_R as the auxiliary condition sought for independent mass flux calculations.

56

1.7 Discussion of Preliminary Results

At the time of this writing, only independent melt phase results are available, presented in Tables 2 and 3. Comparison can be made between solutions which include bubbles (Table 2) and those which exclude bubbles (Table 3, where gaseous decomposition products are assumed dissolved in the liquid) at three distinct pressures. This comparison clearly shows that for those cases which include bubble formation: (1) The extent of subsurface decomposition is appreciably smaller. (2) The heat feedback at the surface is appreciably larger - within the same range of surface temperatures. Overall melt thickness obtained in both bases was comparable for the same p and T_s-range. A parametric study was run at different values of T_0 as well; the results are withheld due to uncertainties in the corresponding values of the burning rates, which have to be imposed (using experimental data).

Several numerical methods were attempted for the generation of independent gas phase solution manifolds. The quasi-nonsteady approach which was previously used with success [23-25] (in which a parabolic partial differential system is solved by marching in psuedo-time toward steady state) was found too cumbersome in terms of core requirements and CPU time and tended at times to diverge with the diverse kinetics data employed. Direct initial-value methods (marching forth in space from the liquid/gas surface), which are much less costly, are intrinsically divergent, owing to the presence of one set of eigensolutions which diverge as large distance from the surface is attained; this occurs for the logarithmic-transformed system, Eq. (26), as well.

At present, a transform to the ϕ -T plane has been performed to use in a direct (low-cost) initial-value solution for the gas phase system in an iterative mode. This approach is fully formulated, and is expected to overcome the previous numerical difficulties associated with the diverse chemical kinetics scales imposed.

References

1.. Robertson, A. J. B., "The Thermal Decompositon of Explosives,
Part II. Cyclotrimethylenetrinitramine and Cyclotetramethylenetetranitramine
and Cyclotetramethylenetetranitramine," Trans. Faraday Society, No. 45,
pp. 85-93, 1949.

2. Rauch, F. C. and Fanelli, A. J., "The Thermal Decomposition Kinetics of
Hexahydro, 1, 3, 5-trinitro-s-triazine Above the Melting Point:
Evidence for Both a Gas and Liquid Phase Decomposition," The Journal
of Physical Chemistry, Vol. 73, No. 5, May 1969, pp. 1604-1608.

3. Rogers, R. N. and Smith, L. C., "Application of Scanning Calorimetry
to the Study of Chemical Kinetics," Thermochimica Acta, No. 1, 1970,
pp. 1-9.

4. Rogers, R.N., "Differential Scanning Calorimetric Determination of
Kinetic Constants of Systems that Melt with Decomposition," Thermochimica
Acta 3, 1972, pp. 437-447.

5. Roger, R. N. and Daub, G. W., "Scanning Calorimetric Determination
of Vapor-Phase Kinetic Data," Analytical Chemistry, Vol. 45 pp. 596-600,
March 1973.

6. Rogers, R. N., "Determination of Condensed Phase Kinetic Constants,"
Note, Thermochimica Acta, No. 9, pp, 444-446, 1974.

7. Suryanarayana, B., Graybush, R. J. and Autera, J. R. "Thermal Degradation
of Secondary Nitramines: A Nitrogen-1 Tracer Study of HMX (1, 3, 5, 7
Tetranitro-1, 3, 5, 7- Tetraazacyclooctane)," Chemistry and Industry, pp.
2177-2178, December 30, 1967.

8. McCarty, K. P., "HMX Propellant Combustion Studies: Phase 1, Literature
Search and Data Assessment," AFRPL-TR-76-59, December, 1976.

9. Cosgrove, J. D. and Owen, A. J., "The Thermal Decomposition of 1, 3, 5
Trinitrohexadydro-1, 3, 5 triazine (RDX)," Chemical Communications,
1968, p. 286.

10. Cosgrove, J. D. and Owen, A. J., "The Thermal Decomposition of 1, 3,
5 Trinitro Hexahydro 1, 3, 5 Triazine (RDX) Part I The Products and
Psysical Parameters," Combustion and Flame, No. 22, 1974, pp. 13-18.

11. Cosgrove, J. D. and Owen, A. J., "The Thermal Decomposition of 1,
3, 5 Trinitro Hexahydro 1, 3, 5 Triazine (RDX) Part II: The Effects
of the Products," Combustion and Flame, No. 22, 1974, pp. 19-22.

12. Rogers, R. N. and Morris, E. D., "On Estimating Activations Energies
with a Differential Scanning Calorimeter," Analitical Chemistry, Vol.
38 (1966), pp. 412-414.

13. Pollard, F. H. and Wyatt, R. M. H., "Reactions Between Formaldehyde and Nitrogen Dioxide. Part I: The Kinetics of the Slow Reaction," Trans. Faraday Society, Vol. 45, 1949, pp. 760-767.

14. Pollard, F. H. and Woodward, P., "Reactions Between Formaldehyde and Nitrogen Dioxide. Part II: The Explosive Reaction," Trans. Faraday Society 45, 1949, pp. 767-770.

15. Pollard, F. H. and Wyatt, R. M. H., "Reactions Between Formaldehyde and Nitrogen Dioxide. Part III: The Determination of Flame Speeds," Trans. Faraday Society 46, 1950, pp. 281-289.

16. Goshgarian, B. B., "The Decompositon of Cyclotrimethylenetrinitramine (RDX) and Cyclotetramethylenetetranitramine," AFRPL-TR-78-76, October 1978.

17. Brenecker, R. R. and Smith, L. C., "On the Products Formed in the Combustion of Explosives. Freeze Out of the Water-Gas Reaction," Journal of Physical Chemistry, 71, No. 8, 1967, pp. 2381-2390.

18. Rocchio, J. J. and Juhasz, A. A., "HMX Thermal Decomposition Chemistry and Its Relation to HMX-Composite Propellant Combustion," 11th JANNAF Combustion Meeting, CPIA Publication No. 261, December 1974, pp. 247-265.

19. Lenchitz, C. and Velicky, R. W., "The Role of Thermochemistry in HMX Propellant Burning," 12th JANNAF Combustion Meeting, CPIA Publication 273, Vol. II, Dec. 1975. pp. 301-321.

20. Shaw, R. and Walker, F. E., "Estimated Kinetics and Thermochemistry of Some Initial Unimolecular Reactions in the Thermal Decompositon of 1, 3, 5, 7 Tetranitro-1, 3, 5, 7 tetraazacyclooctane in the Gas Phase," The Journal of Physical Chemistry, Vol. 81, No. 25, pp. 2572-2576, 1977.

21. Fifer, R., "Shock Tube Study of the High Temperature Kinetics and Mechanism of Nitrogen Dioxide - Aldehyde Reactions," Modern Development in Shock Tube Research, Proc. 10th International Shock tube Symposium, Kyoto, Japan, 1975, pp. 613-620.

22. Fogelzang, A. E., Svetlov, B. S., Azhemian, V. Ya. Kolyasov, S. M. and Sergienko, O. I., "The Combustion of Nitramines and Nitosamines," Translated from Docladi Academi Nauk, SSSR, Bol. 216, No. 3 May 1974, pp. 603-606.

23. BenReuven, M., "Nitramine Monopropellant Deflagration and Nonsteady, Reacting Rocket Chamber Flows," Ph.D. Thesis, No. 1455-T Dept of Mechanical and Aerospace Engineering, Princeton University, Princeton, NJ November 1979.

24. BenReuven, M., Caveny. L.H., Vichnevetsky, R, and Summerfield, M., "Flame Zone and Subsurface Reaction Model for Deflagrating RDX," Proceedings, 16th Symposium (International) on Combustion, The Combustion Institute, Pittsburgh, PA, 1976, pp 1223-1233.

25. BenReuven, M. and Caveny, L.H., "Nitramine Flame Chemistry and Deflagration Interpreted in Terms of a Flame Model,"AIAA Jour. Vol. 19, No. 10, Oct. 1981, pp. 1276-1285.

26. Schroeder, M.A. "Critical Analysis of Nitramine Decomposition Results: Some Comments on Chemical Mechanism,"Proc. 16th JANNAF Combustion Meeting, CPIA Pub. No. 308, Vol. II, Dec. 1979, pp. 17-34

27. Schroeder, M.A. "Critical Analysis of Nitramine Decomposition Data: Activation Energies and Frequency Factors for HMX and RDX,"Proc. 17th JANNAF Combustion Meeting, CPIA Pub. 329, Sep. 1980, Vol. II, pp. 403-508.

28. Schroeder, M.A. "Critical Analysis of Nitramine Decomposition Data: Product Distributions from HMX and RDX,"Proc. JANNAF Combustion Meeting, CPIA Pub. 347, Oct. 1981, Vol. II, pp. 395-413.

29. McGuire, R.R., and Traver, C.M. "Chemical Decomposition Models for the Thermal Explosion of Confined HMX, TATB, RDX, and TNT Explosives," Proc. 7th Detonation Symposium (International), Annalpolis MD, June 1981, pp. 550-557.

30. Beyer, R.A., and Morgan, C.U. "Electron Spin Resonance Studies of HMX and RDX Decomposition,"Proc. 16th JANNAF Combustion Meeting, CPIA Pub. 308, Dec. 1979, Vol. II, pp. 51-57
    also, cf
    Pough, H.L. Davis, L.P., Wilkes, J.S., Carper, W.R., and Dorey, R.C. "Thermal Decomposition of RDX Below the Melting Point,"Proc. 7th Symposium (International) on Detonation, Annapolis, MD, June 1981, pp. 45-52.
    also, cf
    Axworthy, A.E., Flanagan, J.E., Woolery, D.O. "High Temperature Pyrolysis Studies of HMX, RDX and TAGN,"Proceedings, 15th JANNAF Combustion Meeting, CPIA Pub. 297, Sept. 1978, pp. 253-265.

31 Farber, M. and Srivastava, R.D. "Thermal Decomposition of HMX," Proceedings, 16th JANNAF Combustion Meeting, CPIA Publication 308 Dec. 1979 Vol. II, pp. 59-71.

32. Fifter, R.A. and Holmes, H.E., "Kinetics of Nitramine Flame Reactions," Proceedings, 16th JANNAF Combustion Meeting, CPIA Pub. 308 September, 1979, Vol. II, pp. 35-50.

33. Derr, R. L., Boggs, T. L., Zurn, D. E. and Dibble, E. J., "The Combustion Characteristics of HMX," 11th JANNAF Combustion Meeting, CPIA Publication 261, Vol 1, Dec. 1974, pp. 231-241.

34. Nigmatulin, R.I. "Methods of Mechanics of a Continuous Medium for the Description of Multiphase Mixtures,"PMM Vol. 34, No. 6, 1970, pp. 1097-1112 (TRANS.)

35. Williams, F. A., Combustion Theory, Addison-Wesley, Reading, Mass., 1965, Chapter 1: "Summary of Basic Fluid Dynamics and Chemical Kinetics," pp. 1-17.

36. Scala, S. M. and Sutton, G.W., "Energy Transfer at a Chemically Reacting or Slip Interface," ARS Journal, Feb. 1959, pp. 141-143.

37. Plesset, M.S. and Prosperetti, A., "Bubble Dynamics and Cavitation," Annual Reviews, Fluid Mechanics, 9, 1977, pp. 145-185.

TABLE 1

CHEMICAL KINETICS RATE DATA - BASEPOINT

REACTION	APP. ORDER	A	E(kcal/mol)	SOURCE
(L) RDX(L) DECOMP.	1	3×10^{18}	47.5	Robertson
(1) RDX(6) DECOMP.	1	3.55×10^{15}	41.5	Robertson
(2) $CH_2O + NO_2$	2	10^6	19.	Pollard
(3) $CH_2O + N_2O$	2	8.41×10^{11}	27.4	Fifer*
(4) $CH_2O + NO$	2	$2 \times 10^3 . RuT$	70.	Penner**
(5) $CO + H_2O$	2	1.5×10^{13}	52.9	Valance
(6) $CO_2 + H_2$	2	2.68×10^{14}	58.48	Valance

NOTES: A (1/s) For first order, and $(m^3/mol-s)$ for second order
*) somewhat modified: termolecular dependence not considered
**) kinetics originally for NO + aniline, adopted

62

TABLE 2.a RDX MELT WITH GAS BUBBLES

$T_0 = 300$ K, $p = 2$ MPA m $= 8.76$ kg/m^2-s

++CONDENSED PHASE PROFILES++

J	TEMP(K)	DMLSS.TEMP	YNTR	Y,MICRONS	KDT/DY,J/M2-S	RHOB,KG/M3
1	0.4785E+03	0.0	0.1000E+01	0.0	0.4351E+07	0.1820E+04
2	0.4879E+03	0.4000E-01	0.1000E+01	0.6250E+00	0.4506E+07	0.1820E+04
3	0.4974E+03	0.8000E-01	0.1000E+01	0.1229E+01	0.4662E+07	0.1820E+04
4	0.5068E+03	0.1200E+00	0.1000E+01	0.1813E+01	0.4818E+07	0.1820E+04
5	0.5163E+03	0.1600E+00	0.1000E+01	0.2378E+01	0.4974E+07	0.1820E+04
6	0.5257E+03	0.2000E+00	0.1000E+01	0.2926E+01	0.5130E+07	0.1820E+04
7	0.5352E+03	0.2400E+00	0.1000E+01	0.3457E+01	0.5285E+07	0.1820E+04
8	0.5446E+03	0.2800E+00	0.1000E+01	0.3973E+01	0.5441E+07	0.1820E+04
9	0.5541E+03	0.3200E+00	0.1000E+01	0.4475E+01	0.5597E+07	0.1820E+04
10	0.5635E+03	0.3600E+00	0.1000E+01	0.4962E+01	0.5752E+07	0.1820E+04
11	0.5730E+03	0.4000E+00	0.1000E+01	0.5437E+01	0.5906E+07	0.1820E+04
12	0.5824E+03	0.4400E+00	0.1000E+01	0.5900E+01	0.6059E+07	0.1819E+04
13	0.5919E+03	0.4800E+00	0.1000E+01	0.6351E+01	0.6210E+07	0.1818E+04
14	0.6013E+03	0.5200E+00	0.1000E+01	0.6791E+01	0.6357E+07	0.1816E+04
15	0.6108E+03	0.5600E+00	0.1000E+01	0.7222E+01	0.6496E+07	0.1812E+04
16	0.6202E+03	0.6000E+00	0.9999E+00	0.7644E+01	0.6621E+07	0.1806E+04
17	0.6297E+03	0.6400E+00	0.9999E+00	0.8058E+01	0.6724E+07	0.1795E+04
18	0.6391E+03	0.6800E+00	0.9998E+00	0.8468E+01	0.6790E+07	0.1775E+04
19	0.6486E+03	0.7200E+00	0.9997E+00	0.8875E+01	0.6793E+07	0.1743E+04
20	0.6580E+03	0.7600E+00	0.9995E+00	0.9284E+01	0.6698E+07	0.1690E+04
21	0.6675E+03	0.8000E+00	0.9991E+00	0.9704E+01	0.6453E+07	0.1604E+04
22	0.6769E+03	0.8400E+00	0.9984E+00	0.1015E+02	0.5988E+07	0.1472E+04
23	0.6864E+03	0.8800E+00	0.9971E+00	0.1064E+02	0.5227E+07	0.1277E+04
24	0.6958E+03	0.9200E+00	0.9946E+00	0.1123E+02	0.4111E+07	0.1006E+04
25	0.7053E+03	0.9600E+00	0.9886E+00	0.1206E+02	0.2661E+07	0.6633E+03
26	0.7147E+03	0.1000E+01	0.9648E+00	0.1366E+02	0.1028E+07	0.2831E+03

J	HTOT,J/M2-S	DTAU/DZ	UG,M/S	PSI=VG/V	KB/K(LIQ)
1	0.8078E+07	0.1117E+01	0.5003E+00	0.0	0.1000E+01
2	0.8234E+07	0.1157E+01	0.5102E+00	0.0	0.1000E+01
3	0.8390E+07	0.1197E+01	0.5201E+00	0.0	0.1000E+01
4	0.8546E+07	0.1237E+01	0.5299E+00	0.0	0.1000E+01
5	0.8701E+07	0.1277E+01	0.5398E+00	0.0	0.1000E+01
6	0.8857E+07	0.1317E+01	0.5497E+00	0.0	0.1000E+01
7	0.9013E+07	0.1357E+01	0.5596E+00	0.0	0.1000E+01
8	0.9169E+07	0.1397E+01	0.5695E+00	0.0	0.1000E+01
9	0.9324E+07	0.1437E+01	0.5793E+00	0.0	0.1000E+01
10	0.9479E+07	0.1476E+01	0.5892E+00	0.1163E-03	0.9999E+00
11	0.9634E+07	0.1516E+01	0.5991E+00	0.2372E-03	0.9998E+00
12	0.9787E+07	0.1555E+01	0.6090E+00	0.6025E-03	0.9995E+00
13	0.9938E+07	0.1594E+01	0.6188E+00	0.1102E-02	0.9991E+00
14	0.1008E+08	0.1632E+01	0.6287E+00	0.2237E-02	0.9981E+00
15	0.1022E+08	0.1667E+01	0.6386E+00	0.4284E-02	0.9964E+00
16	0.1035E+08	0.1700E+01	0.6485E+00	0.7778E-02	0.9935E+00
17	0.1045E+08	0.1726E+01	0.6584E+00	0.1402E-01	0.9882E+00
18	0.1052E+08	0.1743E+01	0.6682E+00	0.2467E-01	0.9793E+00
19	0.1052E+08	0.1744E+01	0.6781E+00	0.4259E-01	0.9642E+00
20	0.1042E+08	0.1719E+01	0.6880E+00	0.7211E-01	0.9394E+00
21	0.1018E+08	0.1656E+01	0.6979E+00	0.1194E+00	0.8997E+00
22	0.9709E+07	0.1537E+01	0.7078E+00	0.1925E+00	0.8382E+00
23	0.8943E+07	0.1342E+01	0.7176E+00	0.3005E+00	0.7474E+00
24	0.7819E+07	0.1055E+01	0.7275E+00	0.4502E+00	0.6215E+00
25	0.6346E+07	0.6830E+00	0.7374E+00	0.6394E+00	0.4625E+00
26	0.4625E+07	0.2640E+00	0.7473E+00	0.8499E+00	0.2855E+00

TABLE 2.b RDX MELT WITH GAS BUBBLES

$T_0 = 300$ K, $p = 6$ MPa, $m = 19.7$ kg/m²-s

++CONDENSED PHASE PROFILES++

J	TEMP(K)	DMLSS.TEMP	YNTR	Y,MICRONS	KDT/DY,J/M2-S	RHOB,KG/M3
1	0.4785E+03	0.0	0.1000E+01	0.0	0.9792E+07	0.1820E+04
2	0.4894E+03	0.4000E-01	0.1000E+01	0.3183E+00	0.1020E+08	0.1820E+04
3	0.5002E+03	0.8000E-01	0.1000E+01	0.6243E+00	0.1060E+08	0.1820E+04
4	0.5111E+03	0.1200E+00	0.1000E+01	0.9189E+00	0.1100E+08	0.1820E+04
5	0.5219E+03	0.1600E+00	0.1000E+01	0.1203E+01	0.1140E+08	0.1820E+04
6	0.5328E+03	0.2000E+00	0.1000E+01	0.1477E+01	0.1181E+08	0.1820E+04
7	0.5437E+03	0.2400E+00	0.1000E+01	0.1742E+01	0.1221E+08	0.1820E+04
8	0.5545E+03	0.2800E+00	0.1000E+01	0.1998E+01	0.1261E+08	0.1820E+04
9	0.5654E+03	0.3200E+00	0.1000E+01	0.2246E+01	0.1302E+08	0.1820E+04
10	0.5762E+03	0.3600E+00	0.1000E+01	0.2487E+01	0.1342E+08	0.1820E+04
11	0.5871E+03	0.4000E+00	0.1000E+01	0.2721E+01	0.1382E+08	0.1820E+04
12	0.5980E+03	0.4400E+00	0.1000E+01	0.2947E+01	0.1422E+08	0.1819E+04
13	0.6088E+03	0.4800E+00	0.1000E+01	0.3168E+01	0.1462E+08	0.1819E+04
14	0.6197E+03	0.5200E+00	0.1000E+01	0.3383E+01	0.1500E+08	0.1817E+04
15	0.6305E+03	0.5600E+00	0.9999E+00	0.3592E+01	0.1538E+08	0.1815E+04
16	0.6414E+03	0.6000E+00	0.9999E+00	0.3797E+01	0.1573E+08	0.1810E+04
17	0.6523E+03	0.6400E+00	0.9998E+00	0.3997E+01	0.1604E+08	0.1801E+04
18	0.6631E+03	0.6800E+00	0.9996E+00	0.4194E+01	0.1628E+08	0.1786E+04
19	0.6740E+03	0.7200E+00	0.9993E+00	0.4388E+01	0.1639E+08	0.1759E+04
20	0.6848E+03	0.7600E+00	0.9987E+00	0.4583E+01	0.1630E+08	0.1712E+04
21	0.6957E+03	0.8000E+00	0.9977E+00	0.4780E+01	0.1588E+08	0.1636E+04
22	0.7066E+03	0.8400E+00	0.9960E+00	0.4985E+01	0.1498E+08	0.1514E+04
23	0.7174E+03	0.8800E+00	0.9928E+00	0.5209E+01	0.1342E+08	0.1331E+04
24	0.7283E+03	0.9200E+00	0.9865E+00	0.5468E+01	0.1106E+08	0.1072E+04
25	0.7391E+03	0.9600E+00	0.9726E+00	0.5803E+01	0.7981E+07	0.7467E+03
26	0.7500E+03	0.1000E+01	0.9235E+00	0.6319E+01	0.4682E+07	0.4004E+03

J	HTOT,J/M2-S	DTRU/DZ	UG,M/S	PSI=VG/V	KB/K(LIQ)
1	0.1818E+08	0.9716E+00	0.3754E+00	0.0	0.1000E+01
2	0.1859E+08	0.1012E+01	0.3839E+00	0.0	0.1000E+01
3	0.1899E+08	0.1052E+01	0.3924E+00	0.0	0.1000E+01
4	0.1939E+08	0.1092E+01	0.4009E+00	0.0	0.1000E+01
5	0.1979E+08	0.1132E+01	0.4094E+00	0.0	0.1000E+01
6	0.2020E+08	0.1172E+01	0.4180E+00	0.0	0.1000E+01
7	0.2060E+08	0.1212E+01	0.4265E+00	0.0	0.1000E+01
8	0.2100E+08	0.1252E+01	0.4350E+00	0.0	0.1000E+01
9	0.2141E+08	0.1291E+01	0.4435E+00	0.0	0.1000E+01
10	0.2181E+08	0.1321E+01	0.4520E+00	0.7915E-04	0.9999E+00
11	0.2221E+08	0.1371E+01	0.4605E+00	0.1619E-03	0.9999E+00
12	0.2261E+08	0.1411E+01	0.4691E+00	0.3300E-03	0.9997E+00
13	0.2301E+08	0.1450E+01	0.4776E+00	0.7136E-03	0.9994E+00
14	0.2339E+08	0.1489E+01	0.4861E+00	0.1495E-02	0.9987E+00
15	0.2377E+08	0.1526E+01	0.4946E+00	0.2909E-02	0.9976E+00
16	0.2412E+08	0.1561E+01	0.5031E+00	0.5594E-02	0.9953E+00
17	0.2443E+08	0.1592E+01	0.5117E+00	0.1048E-01	0.9912E+00
18	0.2466E+08	0.1615E+01	0.5202E+00	0.1923E-01	0.9838E+00
19	0.2477E+08	0.1626E+01	0.5287E+00	0.3447E-01	0.9710E+00
20	0.2468E+08	0.1617E+01	0.5372E+00	0.6039E-01	0.9492E+00
21	0.2425E+08	0.1576E+01	0.5457E+00	0.1032E+00	0.9132E+00
22	0.2334E+08	0.1487E+01	0.5543E+00	0.1713E+00	0.8560E+00
23	0.2175E+08	0.1332E+01	0.5628E+00	0.2741E+00	0.7696E+00
24	0.1934E+08	0.1098E+01	0.5713E+00	0.4187E+00	0.6481E+00
25	0.1614E+08	0.7919E+00	0.5798E+00	0.6009E+00	0.4948E+00
26	0.1251E+08	0.4646E+00	0.5883E+00	0.7946E+00	0.3320E+00

TABLE 2.c RDX MELT WITH GAS BUBBLES

$T_0 = 300$ K, $p = 10$ MPa, $m = 30.2$ kg/m²-s

++CONDENSED PHASE PROFILES++

J	TEMP(K)	DMLSS.TEMP	YNTR	Y,MICRONS	KDT/DY,J/M2-S	RHOB,KG/M3
1	0.4785E+03	0.0	0.1000E+01	0.0	0.1500E+08	0.1820E+04
2	0.4894E+03	0.4000E-01	0.1000E+01	0.2078E+00	0.1562E+08	0.1820E+04
3	0.5002E+03	0.8000E-01	0.1000E+01	0.4076E+00	0.1623E+08	0.1820E+04
4	0.5111E+03	0.1200E+00	0.1000E+01	0.5999E+00	0.1685E+08	0.1820E+04
5	0.5219E+03	0.1600E+00	0.1000E+01	0.7852E+00	0.1747E+08	0.1820E+04
6	0.5328E+03	0.2000E+00	0.1000E+01	0.9642E+00	0.1809E+08	0.1820E+04
7	0.5437E+03	0.2400E+00	0.1000E+01	0.1137E+01	0.1871E+08	0.1820E+04
8	0.5545E+03	0.2800E+00	0.1000E+01	0.1304E+01	0.1932E+08	0.1820E+04
9	0.5654E+03	0.3200E+00	0.1000E+01	0.1466E+01	0.1994E+08	0.1820E+04
10	0.5762E+03	0.3600E+00	0.1000E+01	0.1624E+01	0.2056E+08	0.1820E+04
11	0.5871E+03	0.4000E+00	0.1000E+01	0.1776E+01	0.2117E+08	0.1820E+04
12	0.5980E+03	0.4400E+00	0.1000E+01	0.1924E+01	0.2179E+08	0.1820E+04
13	0.6088E+03	0.4800E+00	0.1000E+01	0.2068E+01	0.2240E+08	0.1819E+04
14	0.6197E+03	0.5200E+00	0.1000E+01	0.2208E+01	0.2301E+08	0.1819E+04
15	0.6305E+03	0.5600E+00	0.1000E+01	0.2345E+01	0.2361E+08	0.1818E+04
16	0.6414E+03	0.6000E+00	0.9999E+00	0.2478E+01	0.2419E+08	0.1816E+04
17	0.6523E+03	0.6400E+00	0.9998E+00	0.2608E+01	0.2475E+08	0.1812E+04
18	0.6631E+03	0.6800E+00	0.9997E+00	0.2735E+01	0.2526E+08	0.1806E+04
19	0.6740E+03	0.7200E+00	0.9995E+00	0.2860E+01	0.2568E+08	0.1794E+04
20	0.6848E+03	0.7600E+00	0.9991E+00	0.2983E+01	0.2597E+08	0.1774E+04
21	0.6957E+03	0.8000E+00	0.9984E+00	0.3105E+01	0.2603E+08	0.1741E+04
22	0.7066E+03	0.8400E+00	0.9973E+00	0.3228E+01	0.2574E+08	0.1686E+04
23	0.7174E+03	0.8800E+00	0.9954E+00	0.3353E+01	0.2492E+08	0.1600E+04
24	0.7283E+03	0.9200E+00	0.9922E+00	0.3485E+01	0.2335E+08	0.1468E+04
25	0.7391E+03	0.9600E+00	0.9863E+00	0.3628E+01	0.2080E+08	0.1277E+04
26	0.7500E+03	0.1000E+01	0.9752E+00	0.3796E+01	0.1717E+08	0.1021E+04

J	HTOT,J/M2-S	DTRU/DZ	UG,M/S	PSI=VG/V	KB/K(LIQ)
1	0.2785E+08	0.9716E+00	0.3450E+00	0.0	0.1000E+01
2	0.2847E+08	0.1012E+01	0.3528E+00	0.0	0.1000E+01
3	0.2909E+08	0.1052E+01	0.3606E+00	0.0	0.1000E+01
4	0.2970E+08	0.1092E+01	0.3685E+00	0.0	0.1000E+01
5	0.3032E+08	0.1132E+01	0.3763E+00	0.0	0.1000E+01
6	0.3094E+08	0.1172E+01	0.3841E+00	0.0	0.1000E+01
7	0.3156E+08	0.1212E+01	0.3920E+00	0.0	0.1000E+01
8	0.3217E+08	0.1252E+01	0.3998E+00	0.0	0.1000E+01
9	0.3279E+08	0.1292E+01	0.4076E+00	0.0	0.1000E+01
10	0.3341E+08	0.1331E+01	0.4154E+00	0.2348E-04	0.1000E+01
11	0.3402E+08	0.1371E+01	0.4233E+00	0.7290E-04	0.9999E+00
12	0.3464E+08	0.1411E+01	0.4311E+00	0.1481E-03	0.9999E+00
13	0.3525E+08	0.1451E+01	0.4389E+00	0.3027E-03	0.9997E+00
14	0.3586E+08	0.1490E+01	0.4468E+00	0.6159E-03	0.9995E+00
15	0.3646E+08	0.1529E+01	0.4546E+00	0.1226E-02	0.9990E+00
16	0.3704E+08	0.1567E+01	0.4624E+00	0.2386E-02	0.9980E+00
17	0.3760E+08	0.1603E+01	0.4703E+00	0.4467E-02	0.9962E+00
18	0.3811E+08	0.1636E+01	0.4781E+00	0.8230E-02	0.9931E+00
19	0.3853E+08	0.1663E+01	0.4859E+00	0.1480E-01	0.9876E+00
20	0.3881E+08	0.1682E+01	0.4937E+00	0.2606E-01	0.9781E+00
21	0.3886E+08	0.1686E+01	0.5016E+00	0.4501E-01	0.9622E+00
22	0.3856E+08	0.1667E+01	0.5094E+00	0.7597E-01	0.9361E+00
23	0.3772E+08	0.1614E+01	0.5172E+00	0.1251E+00	0.8949E+00
24	0.3610E+08	0.1512E+01	0.5251E+00	0.2000E+00	0.8319E+00
25	0.3347E+08	0.1347E+01	0.5329E+00	0.3082E+00	0.7409E+00
26	0.2970E+08	0.1112E+01	0.5407E+00	0.4531E+00	0.6191E+00

TABLE 3.a RDX MELT W/OUT BUBBLES

$T_0 = 300$ K, p = 2 Mpa, M = 8,76 kg/m^2-s

++CONDENSED PHASE PROFILES++

J	TEMP(K)	DMLSS.TEMP	YNTR	.MICRONS	KDT/DY,J/M2-S
1	0.4785E+03	0.0	0.1000E+01	0.0	0.4351E+07
2	0.4874E+03	0.4000E-01	0.1000E+01	0.5896E+00	0.4497E+07
3	0.4963E+03	0.8000E-01	0.1000E+01	0.1160E+01	0.4644E+07
4	0.5052E+03	0.1200E+00	0.1000E+01	0.1713E+01	0.4791E+07
5	0.5141E+03	0.1600E+00	0.1000E+01	0.2249E+01	0.4938E+07
6	0.5230E+03	0.2000E+00	0.1000E+01	0.2770E+01	0.5085E+07
7	0.5319E+03	0.2400E+00	0.1000E+01	0.3276E+01	0.5232E+07
8	0.5408E+03	0.2800E+00	0.1000E+01	0.3767E+01	0.5378E+07
9	0.5497E+03	0.3200E+00	0.9999E+00	0.4244E+01	0.5525E+07
10	0.5586E+03	0.3600E+00	0.9999E+00	0.4712E+01	0.5672E+07
11	0.5676E+03	0.4000E+00	0.9998E+00	0.5166E+01	0.5818E+07
12	0.5765E+03	0.4400E+00	0.9996E+00	0.5609E+01	0.5963E+07
13	0.5854E+03	0.4800E+00	0.9992E+00	0.6041E+01	0.6106E+07
14	0.5943E+03	0.5200E+00	0.9986E+00	0.6463E+01	0.6248E+07
15	0.6032E+03	0.5600E+00	0.9974E+00	0.6876E+01	0.6385E+07
16	0.6121E+03	0.6000E+00	0.9953E+00	0.7281E+01	0.6514E+07
17	0.6210E+03	0.6400E+00	0.9917E+00	0.7677E+01	0.6630E+07
18	0.6299E+03	0.6800E+00	0.9857E+00	0.8068E+01	0.6726E+07
19	0.6388E+03	0.7200E+00	0.9755E+00	0.8454E+01	0.6786E+07
20	0.6477E+03	0.7600E+00	0.9587E+00	0.8838E+01	0.6790E+01
21	0.6566E+03	0.8000E+00	0.9312E+00	0.9224E+01	0.6704E+07
22	0.6655E+03	0.8400E+00	0.8869E+00	0.9619E+01	0.6475E+07
23	0.6744E+03	0.8800E+00	0.8162E+00	0.1003E+02	0.6021E+07
24	0.6833E+03	0.9200E+00	0.7041E+00	0.1050E+02	0.5216E+07
25	0.6922E+03	0.9600E+00	0.5269E+00	0.1107E+02	0.3858E+07
26	0.7011E+03	0.1000E+01	0.2372E+00	0.1206E+02	0.1545E+07

J	HTOT,J/M2-S	DTAU/DZ
1	0.8078E+07	0.1185E+01
2	0.8225E+07	0.1225E+01
3	0.8372E+07	0.1265E+01
4	0.8519E+07	0.1305E+01
5	0.8666E+07	0.1345E+01
6	0.8812E+07	0.1385E+01
7	0.8959E+07	0.1425E+01
8	0.9106E+07	0.1465E+01
9	0.9252E+07	0.1505E+01
10	0.9399E+07	0.1545E+01
11	0.9544E+07	0.1584E+01
12	0.9689E+07	0.1624E+01
13	0.9831E+07	0.1663E+01
14	0.9970E+07	0.1701E+01
15	0.1010E+08	0.1739E+01
16	0.1022E+08	0.1774E+01
17	0.1033E+08	0.1806E+01
18	0.1040E+08	0.1832E+01
19	0.1042E+08	0.1848E+01
20	0.1036E+08	0.1849E+01
21	0.1018E+08	0.1826E+01
22	0.9781E+07	0.1763E+01
23	0.9063E+07	0.1640E+01
24	0.7841E+07	0.1421E+01
25	0.5822E+07	0.1051E+01
26	0.2429E+07	0.4208E+00

TABLE 3.b RDX MELT W/OUT BUBBLES

$T_0 = 300$ K, p = 6 Mpa, m = 1.97 kg/m^2-s

++CONDENSED PHASE PROFILES++

J	TEMP(K)	DMLSS.TEMP	YNTR	Y,MICRONS	KIT/IY,J/M2-S
1	0.4785E+03	0.0	0.1000E+01	0.0	0.9792E+07
2	0.4891E+03	0.4000E-01	0.1000E+01	0.3121E+00	0.1019E+08
3	0.4998E+03	0.8000E-01	0.1000E+01	0.6123E+00	0.1058E+08
4	0.5104E+03	0.1200E+00	0.1000E+01	0.9015E+00	0.1098E+08
5	0.5211E+03	0.1600E+00	0.1000E+01	0.1180E+01	0.1137E+08
6	0.5317E+03	0.2000E+00	0.1000E+01	0.1450E+01	0.1177E+08
7	0.5424E+03	0.2400E+00	0.1000E+01	0.1710E+01	0.1216E+08
8	0.5530E+03	0.2800E+00	0.1000E+01	0.1963E+01	0.1256E+08
9	0.5636E+03	0.3200E+00	0.1000E+01	0.2207E+01	0.1295E+08
10	0.5743E+03	0.3600E+00	0.9999E+00	0.2444E+01	0.1335E+08
11	0.5849E+03	0.4000E+00	0.9999E+00	0.2674E+01	0.1374E+08
12	0.5956E+03	0.4400E+00	0.9997E+00	0.2898E+01	0.1413E+08
13	0.6062E+03	0.4800E+00	0.9994E+00	0.3116E+01	0.1452E+08
14	0.6169E+03	0.5200E+00	0.9987E+00	0.3328E+01	0.1490E+08
15	0.6275E+03	0.5600E+00	0.9976E+00	0.3534E+01	0.1528E+08
16	0.6381E+03	0.6000E+00	0.9954E+00	0.3736E+01	0.1563E+08
17	0.6488E+03	0.6400E+00	0.9913E+00	0.3933E+01	0.1595E+08
18	0.6594E+03	0.6800E+00	0.9842E+00	0.4127E+01	0.1621E+08
19	0.6701E+03	0.7200E+00	0.9716E+00	0.4318E+01	0.1636E+08
20	0.6807E+03	0.7600E+00	0.9500E+00	0.4509E+01	0.1634E+08
21	0.6914E+03	0.8000E+00	0.9133E+00	0.4701E+01	0.1604E+0
22	0.7020E+03	0.8400E+00	0.8521E+00	0.4899E+01	0.1526E+0
23	0.7126E+03	0.8800E+00	0.7517E+00	0.5114E+01	0.1374E+08
24	0.7233E+03	0.9200E+00	0.5895E+00	0.5364E+01	0.1103E+08
25	0.7339E+03	0.9600E+00	0.3242E+00	0.5719E+01	0.6548E+07
26	0.7446E+03	0.1000E+01	0.4290E-01	0.7402E+01	0.1375E+07

J	HTOT,J/M2-S	DTRU/DZ
1	0.1818E+08	0.9914E+00
2	0.1858E+08	0.1031E+01
3	0.1897E+08	0.1071E+01
4	0.1937E+08	0.1111E+01
5	0.1976E+08	0.1151E+01
6	0.2016E+08	0.1191E+01
7	0.2055E+08	0.1231E+01
8	0.2095E+08	0.1271E+01
9	0.2134E+08	0.1311E+01
10	0.2174E+08	0.1351E+01
11	0.2213E+08	0.1391E+01
12	0.2252E+08	0.1431E+01
13	0.2291E+08	0.1470E+01
14	0.2328E+08	0.1509E+01
15	0.2365E+08	0.1547E+01
16	0.2398E+08	0.1582E+01
17	0.2427E+08	0.1615E+01
18	0.2446E+08	0.1641E+01
19	0.2451E+08	0.1656E+01
20	0.2431E+08	0.1655E+01
21	0.2370E+08	0.1624E+01
22	0.2241E+08	0.1545E+01
23	0.2004E+08	0.1391E+01
24	0.1598E+08	0.1117E+01
25	0.9352E+07	0.6629E+00
26	0.1735E+07	0.1392E+00

TABLE 3.c RDX MELT W/OUT BUBBLES

$$T_0 = 300 \text{ K}, \quad p = 10 \text{ MPa}, \quad m = 30.2 \text{ kg/m}^2\text{-s}$$

++CONDENSED PHASE PROFILES++

J	TEMP-(K)	DMLSS.TEMP	YNTR	Y,MICRONS	KDT/DY,J/M2-S
1	0.4785E+03	0.0	0.1000E+01	0.0	0.1500E+08
2	0.4894E+03	0.4000E-01	0.1000E+01	0.2078E+00	0.1562E+08
3	0.5002E+03	0.8000E-01	0.1000E+01	0.4076E+00	0.1623E+08
4	0.5111E+03	0.1200E+00	0.1000E+01	0.5999E+00	0.1685E+08
5	0.5219E+03	0.1600E+00	0.1000E+01	0.7852E+00	0.1747E+08
6	0.5328E+03	0.2000E+00	0.1000E+01	0.9642E+00	0.1809E+08
7	0.5437E+03	0.2400E+00	0.1000E+01	0.1137E+01	0.1871E+08
8	0.5545E+03	0.2800E+00	0.1000E+01	0.1304E+01	0.1932E+08
9	0.5654E+03	0.3200E+00	0.1000E+01	0.1466E+01	0.1994E+08
10	0.5762E+03	0.3600E+00	0.1000E+01	0.1624E+01	0.2056E+08
11	0.5871E+03	0.4000E+00	0.9999E+00	0.1776E+01	0.2117E+08
12	0.5980E+03	0.4400E+00	0.9998E+00	0.1924E+01	0.2179E+08
13	0.6088E+03	0.4800E+00	0.9997E+00	0.2068E+01	0.2240E+08
14	0.6197E+03	0.5200E+00	0.9994E+00	0.2208E+01	0.2301E+08
15	0.6305E+03	0.5600E+00	0.9987E+00	0.2345E+01	0.2361E+08
16	0.6414E+03	0.6000E+00	0.9976E+00	0.2478E+01	0.2419E+08
17	0.6523E+03	0.6400E+00	0.9955E+00	0.2608E+01	0.2475E+08
18	0.6631E+03	0.6800E+00	0.9917E+00	0.2735E+01	0.2526E+08
19	0.6740E+03	0.7200E+00	0.9851E+00	0.2860E+01	0.2568E+08
20	0.6848E+03	0.7600E+00	0.9736E+00	0.2983E+01	0.2596E+08
21	0.6957E+03	0.8000E+00	0.9541E+00	0.3105E+01	0.2601E+08
22	0.7066E+03	0.8400E+00	0.9215E+00	0.3228E+01	0.2567E+08
23	0.7174E+03	0.8800E+00	0.8678E+00	0.3354E+01	0.2472E+08
24	0.7283E+03	0.9200E+00	0.7810E+00	0.3487E+01	0.2279E+08
25	0.7391E+03	0.9600E+00	0.6424E+00	0.3638E+01	0.1938E+08
26	0.7500E+03	0.1000E+01	0.4313E+00	0.3829E+01	0.1379E+08

J	HTOT,J/M2-S	DTAU/DZ
1	0.2785E+08	0.9716E+00
2	0.2847E+08	0.1012E+01
3	0.2909E+08	0.1052E+01
4	0.2970E+08	0.1092E+01
5	0.3032E+08	0.1132E+01
6	0.3094E+08	0.1172E+01
7	0.3156E+08	0.1212E+01
8	0.3217E+08	0.1252E+01
9	0.3279E+08	0.1292E+01
10	0.3341E+08	0.1331E+01
11	0.3402E+08	0.1371E+01
12	0.3464E+08	0.1411E+01
13	0.3525E+08	0.1451E+01
14	0.3585E+08	0.1490E+01
15	0.3644E+08	0.1529E+01
16	0.3701E+08	0.1567E+01
17	0.3754E+08	0.1603E+01
18	0.3800E+08	0.1636E+01
19	0.3834E+08	0.1663E+01
20	0.3847E+08	0.1682E+01
21	0.3827E+08	0.1685E+01
22	0.3751E+08	0.1663E+01
23	0.3587E+08	0.1601E+01
24	0.3283E+08	0.1476E+01
25	0.2765E+08	0.1255E+01
26	0.1933E+08	0.8931E+00

NARROW NEAR-FIELD REGION:
HIGH GRADIENTS
CONVECTIVE-DIFFUSIVE-REACTIVE

TEMPERATURE

T_F

T_s

WIDE FAR-FIELD REGION:
LOW GRADIENTS
CONVECTIVE-REACTIVE

MASS FRACTIONS & TEMPERATURE

Y_{NO_2}

Y_{NTR}

Y

$LOG(\omega_1)$

FAR FIELD: SECONDARY
REACTIONS DOMINATE

REACTION RATE

$LOG(\omega_2)$,
E.G.,
$NO_2 + CH_2O$

NEAR FIELD:
NITRAMINE
DECOMPOSITION
DOMINANT

0^+

DISTANCE FROM PROPELLANT SURFACE

Y
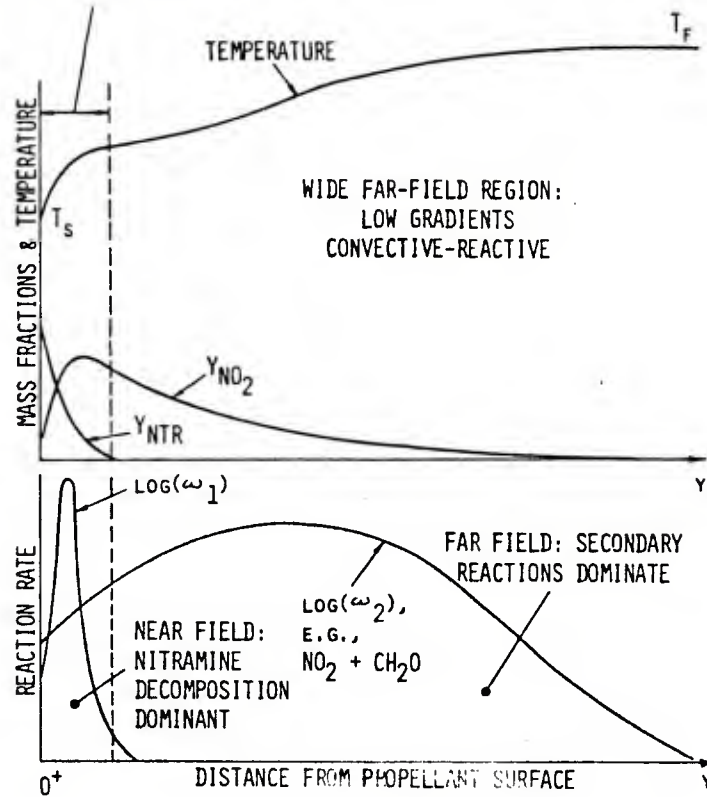
Fig. 1. Schematic of the nitramine
gaseous flame field, showing the near-
field and far-field concepts.
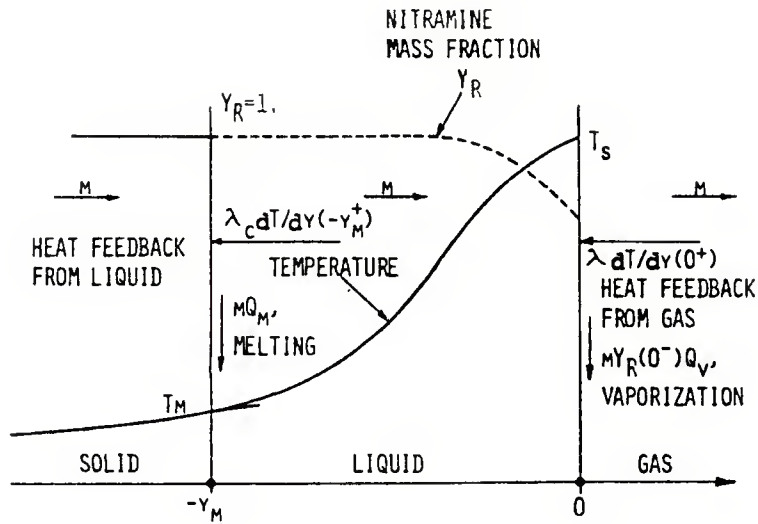
Fig. 2. Schematic of the condensed phase with decomposition. Gaseous bubbles (decomposition products) become prominent as the nitramine mass fraction drops.

APPENDIX A

CONDENSED-PHASE DECOMPOSITION
FOR A DEFLAGRATING SOLID PROPELLANT

Appendix A
Condensed-Phase Decomposition
for a Deflagrating Solid Propellant

Two distinct cases involving condensed-phase decomposition of deflagrating monopropellants are treated herein in a highly approximate manner. The objective is to obtain simple analytical expressions for the extent of decomposition (remaining mass fraction of reactant) and the thermal gradient at the surface. In the first case, assumed to represent nitramines, the extent of subsurface reaction is expected to be small. In the second case, assumed applicable to AP, the extent of subsurface decomposition expected is relatively large. In both instances, the associated activation energies are assumed relatively high, and the process exothermic overall.

1. Nitramine-like Subsurface Decomposition

A single, first-order-overall reaction is considered, which is consistent with the observations of Robertson [37] on condensed-phase decomposition of nitramines. The physical model and coordinate system are depicted in Fig. A.1.

A liquid phase near the surface is assumed, where all subsurface decomposition occurs. Two characteristic features are assumed: (1) only a small extent of decomposition - up to 15% reactant depletion within the pressure range 1-10 MPa, and (2) The melting temperature, T_m, is sufficiently smaller than typical surface temperatures. As a consequence of (2) and the high activation energy, E_c, most of the reaction would occur in a thin region within the liquid phase, under temperatures close to T_s. Note also that all products of decomposition are gaseous, and are assumed dissolved in the liquid.

Let the dimensionless thermal enthalpy and the length coordinate be defined,

$$\tau \equiv (T-T_0)/(T_s-T_0), \quad z \equiv y/(\lambda_c/mC_c) \quad \text{(A.1)}$$

The associated conservation equations for the region of the liquid phase, $z_m < z < 0$:

$$\tau' - \tau'' = K_c^* e^{-f(\tau)/\varepsilon} \gamma \quad \text{(A.2)}$$

$$\gamma' = -K_c e^{-f(\tau)/\varepsilon} \gamma \quad \text{(A.3)}$$

where:
$$K_c \equiv \frac{\lambda_c}{C_c} A_c \rho_c e^{-1/\varepsilon} / m^2 \sim O(1) \quad \text{(A.4)}$$

73

$$K_c^* \equiv K_c Q_L^* / C_c (T_s - T_0) \qquad \text{(A.5)}$$

$$0 < \varepsilon \equiv T_s / \beta_c \ll 1 \qquad \text{(A.6)}$$

$$f(\tau)/\varepsilon = \frac{1}{\varepsilon}(1-\tau)/(\tau + a_1), \quad a_1 \equiv T_s / (T_s - T_0) \qquad \text{(A.7)}$$

and $Y(z)$ denotes the reactant mass fraction.

The associated boundary data are:

$$Y(z_m) = 1 \qquad \text{(A.8)}$$

$$\tau(z_m) = \tau_m = \frac{T_m - T_0}{T_s - T_0}, \quad \tau(0) = 1 \qquad \text{(A.9)}$$

$$\tau(z_m) - \tau'(z_m) = -q_m \qquad \text{(A.10)}$$

where $q_m \equiv Q_m^* / C_c (T_s - T_0)$.

The last condition in Eq. (A.10) arises due to energy conservation at the liquid/solid interface, where Q_m^*, the heat of melting, is depleted.

The system can now be conveniently transformed, using as the independent variable, for $\tau_m < \tau < 1$:

$$(\tau - \phi) \, d\phi/d\tau = K_c^* \, e^{-f(\tau)/\varepsilon} Y \qquad \text{(A.11)}$$

$$(\tau - \phi) \, dY/d\tau = -K_c \, e^{-f(\tau)/\varepsilon} Y \qquad \text{(A.12)}$$

where $\phi(\tau) \equiv \tau - \tau'$ and $Y = Y(\tau)$. The associated boundary conditions are

$$\phi(\tau_m) = -q_m, \quad Y(\tau_m) = 1 \qquad \text{(A.13)}$$

As stated earlier, most of the chemical reaction is expected to occur in a thin, high-temperature region near the surface, where $\tau \sim 1$. Thus, the quantity $0 < \varepsilon \ll 1$ is suggested as a small perturbation parameter, and the τ-domain is conceived to have a narrow boundary-layer (or "inner") region, where chemical reaction is important; over the rest of the liquid phase (or "outer" region), the reaction is negligible.

Sufficient resolution for the inner region is obtained by use of the stretched coordinate,

$$\eta \equiv (1-\tau)/\varepsilon \qquad \text{(A.14)}$$

Thus, transforming to the inner variables $\overline{\Phi}$, $\overline{\Upsilon}$ and η, the conservation equations are

$$(1-\phi-\varepsilon\eta)\,d\overline{\Phi}/d\eta = -\varepsilon K_c^* e^{-F(\eta)}\overline{\Upsilon} \qquad \text{(A.15)}$$

$$(1-\phi-\varepsilon\eta)\,d\overline{g}/d\eta = +\varepsilon K_c\, e^{-F(\eta)} \qquad \text{(A.16)}$$

where
$$F(\eta) \equiv \frac{\eta/a_1}{1-\varepsilon\eta/a_1} \sim \frac{\eta}{a_1}\Big[1 + \varepsilon(\tfrac{\eta}{a_1}) + \cdots\Big]$$

The following inner expansions are suggested, in simple powers of ε:

$$\overline{\Phi}(\eta) \sim \overline{\Phi}_0(\eta) + \varepsilon\overline{\Phi}_1(\eta) + \varepsilon^2\overline{\Phi}_2(\eta) + \cdots \qquad \text{(A.17)}$$

$$\overline{g}(\eta) \equiv \ln\overline{\Upsilon}(\eta) \sim \overline{g}_0(\eta) + \varepsilon\overline{g}_1(\eta) + \varepsilon^2\overline{g}_2(\eta) + \cdots \qquad \text{(A.18)}$$

The exponential term is likewise expanded:

$$e^{-F(\eta)} \sim e^{-\eta/a_1}\Big[1 + \varepsilon(\tfrac{\eta}{a_1})^2 + \varepsilon^2(\tfrac{\eta}{a_1})^3 + \cdots\Big] \qquad \text{(A.19)}$$

Substitution of these series expansions into the inner conservation equations (A.15) and (A.16) results in an ordered hierarchy of differential systems after collecting terms in equal powers of ε:

Zeroth order:

$$(1-\overline{\Phi}_0)\,d\overline{\Phi}_0/d\eta = 0, \quad \overline{\Phi}_0(0) = C_0 \qquad \text{(A.20a)}$$

$$(1-\overline{\Phi}_0)\,d\overline{g}_0/d\eta = 0, \quad \overline{g}_0(0) = 0 \qquad \text{(A.20b)}$$

with the solutions

$$\overline{\Phi}_0(\eta) = C_0 = \text{const}, \quad \overline{g}_0(\eta) = 0 . \qquad \text{(A.21)}$$

Recall that according to assumption (1) herein, only a small extent of decomposition is expected. Hence, the boundary condition for $\overline{q}_o$ is homogeneous, leading to a trivial zeroth order solution (implying that $\overline{Y} \sim 1$).

First order:

$$(1-\overline{\Phi}_o)\frac{d\overline{\Phi}_1}{d\eta} - \eta\frac{d\overline{\Phi}_o}{d\eta} = -K_c^* e^{-\eta/a_1}, \quad \overline{\Phi}_1(0) = C_1 \quad \text{(A.22a)}$$

$$(1-\overline{\Phi}_o)\frac{d\overline{q}_1}{d\eta} - \eta\frac{d\overline{q}_o}{d\eta} = K_c e^{-\eta/a_1}, \quad \overline{q}_1(0) = b_1 \quad \text{(A.22b)}$$

Note that now both boundary conditions are inhomogeneous. For the reactant, $\log \overline{Y}(0) \sim O(\varepsilon)$ is expected; accordingly, a defect in the incoming heat flux from the gas (relative to the nonreacting, unperturbed case) must also be anticipated, owing to the slight extent of exothermicity in the condensed phase.

The first order inner solutions are,

$$\overline{\Phi}_1(\eta) = \frac{K_c^* a_1}{1-\overline{\Phi}_o} e^{-\eta/a_1} + \left[C_1 - \frac{K_c^* a_1}{1-\overline{\Phi}_o} \right] \quad \text{(A.23a)}$$

$$\overline{q}_1(\eta) = -\frac{K_c a_1}{1-\overline{\Phi}_o} e^{-\eta/a_1} + \left[b_1 + \frac{K_c a_1}{1-\overline{\Phi}_o} \right] \quad \text{(A.23b)}$$

Solutions of the outer region where $\tau \sim \tau_m$ are generally of the form

$$\phi(\tau) \sim \phi_o(\tau) + e^{-f(\tau)/\varepsilon} \left[\phi_1(\tau) + \varepsilon\phi_2(\tau) + \cdots \right] \quad \text{(A.24)}$$

and likewise for Y (τ). These are similar to the outer-field solutions suggested by Bush and Fendell [29]; detailed calculations and rigorous matching will not be carried out herein. However, important insights can be obtained by inspection. Evidently, the term

$$e^{-f(\tau)/\varepsilon} \ll \varepsilon$$

for typical outer-field values of τ, cf. Eq. (A.7). Thus, the zeroth order solutions are

$$\phi_o(\tau) = -q_m, \quad Y_o(\tau) = 1 \quad \text{(A.25)}$$

determined from Eqs. (A.2), (A.3) and (A.13), using the outer
expansions. The first order outer solutions would obtain exponential
terms analogous to those in Eqs. (A.23), but their boundary data are
homogeneous. Consequently, the square-bracketed constant terms
in Eqs. (A.23) for the inner region have no counterparts in the
outer solutions. This occurs since the small perturbation (due to
reaction near the surface) can not penetrate to the (outer)
liquid/solid boundary.

Therefore, the present approximation can be concluded by imposing

$$C_1 = K_c^* a_1 / (1 - \overline{\Phi}_o) + O(\varepsilon) \qquad \text{(A.26)}$$

$$b_1 = - K_c a_1 / (1 - \overline{\Phi}_o) + O(\varepsilon) \qquad \text{(A.27)}$$

while $\overline{\Phi}_o = \Phi_o = -q_m$, all of which arise due to inner-outer matching
requirements.

The important consequences of Eqs. (A.26), (A.27) are that the
values of the mass fraction of remaining reactant G and the
dimensionless thermal gradient $\tau'(0)$ can be defined at the surface:

$$g(0) = \overline{g}_o(0) + \varepsilon \overline{g}_1(0) = \varepsilon b_1 = - \varepsilon \frac{K_c a_1}{1 + q_m} + O(\varepsilon^2)$$

$$G(T_s, m; T_o) = \exp\left[- \varepsilon \frac{K_c a_1}{1 + q_m}\right] \qquad \text{(A.28)}$$

Similarly,

$$\tau'(0) = 1 - \Phi(0) = 1 - \left(\overline{\Phi}_o(0) + \varepsilon \overline{\Phi}_1(0)\right) = 1 + q_m - \varepsilon \frac{K_c^* a_1}{1 + q_m} + O(\varepsilon^2)$$

Now, since $e^{-x} = 1 - x + O(x^2)$ for $x \ll 1$, the last equality may be
rewritten in terms of G:

$$\tau'(0) = (1 + q_m) - (1 - G) Q_c^* / c_c (T_s - T_o) \qquad \text{(A.29)}$$

The explicit expression obtained for G enables now calculations of
the burning rate (using the eigenvalue equation), as well as n(p)
and $\sigma_p(p)$, where partial derivatives of ln(G) with respect to m,
T_s, and T_o are required.
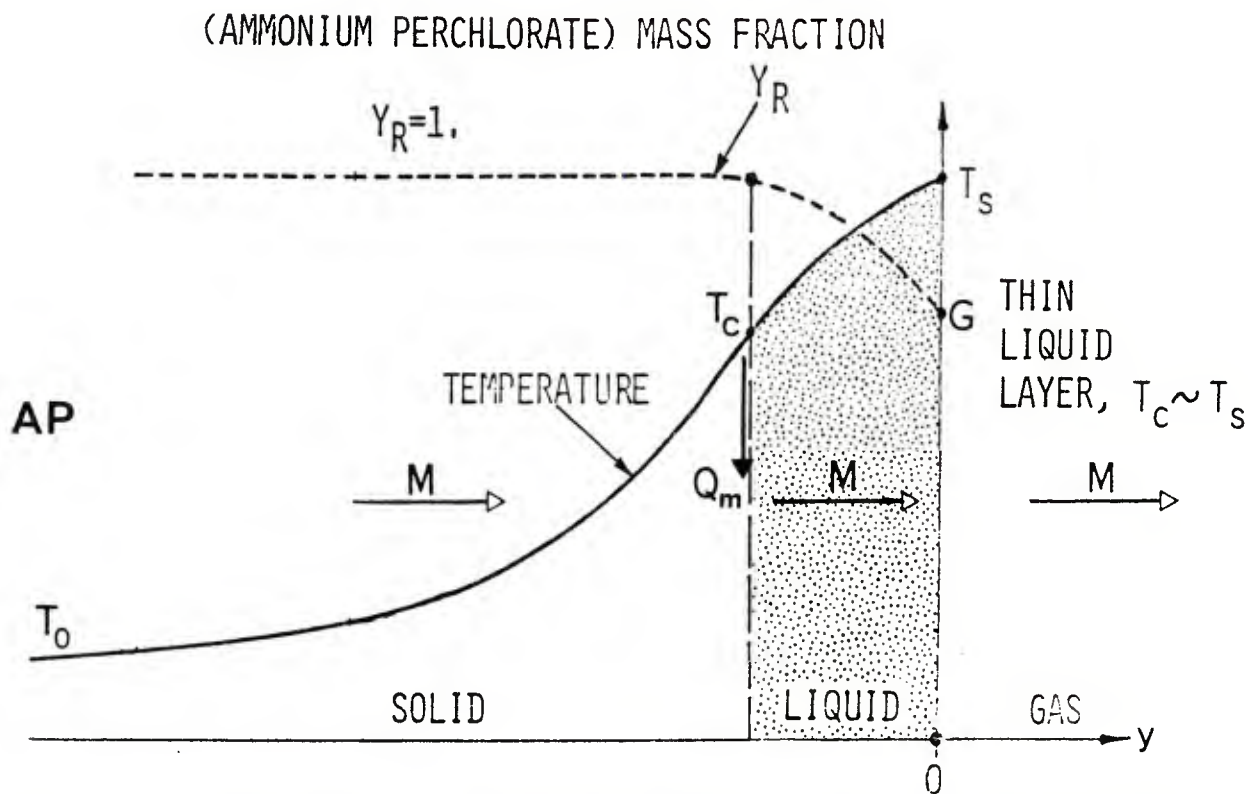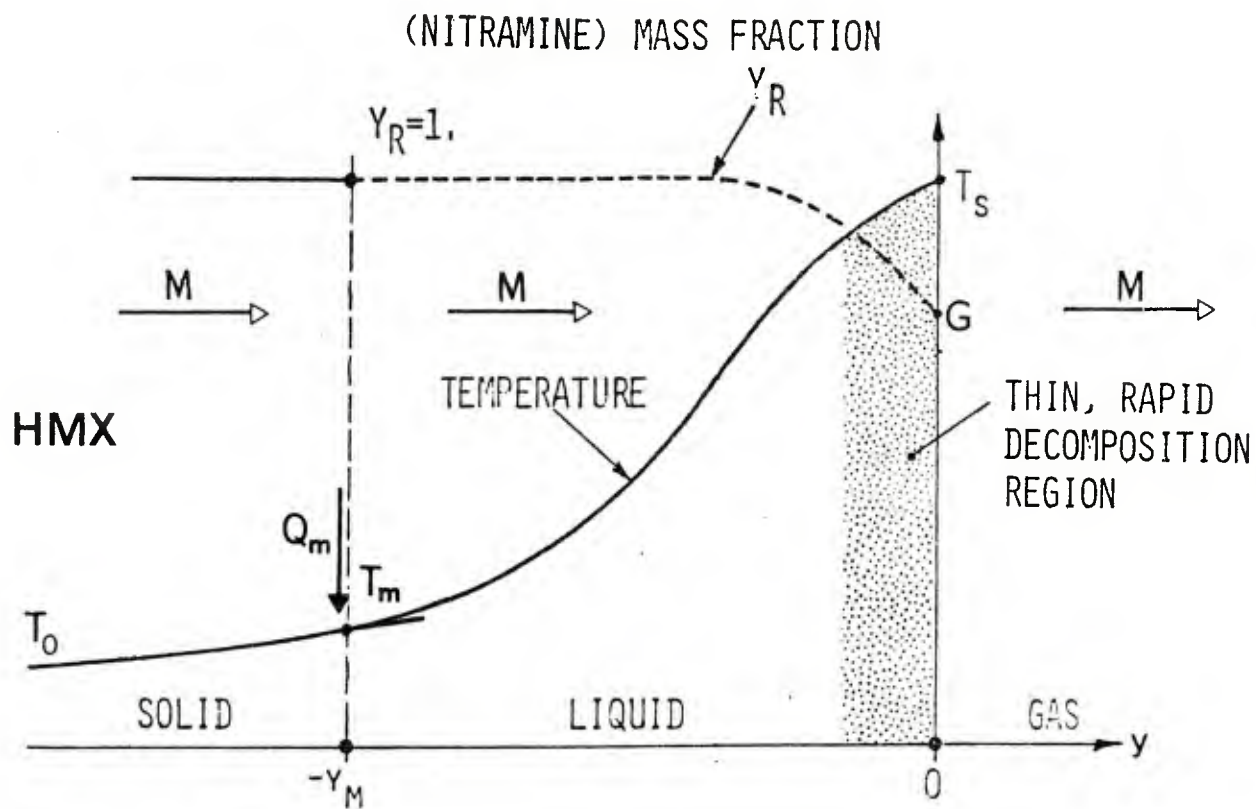
Fig. A. 1 Schematic diagrams of condensed-phase processes described herein for nitramine-like and AP-like monopropellants. In both cases a thin reaction region near the surface prevails due to the high activation energies.

2. Ammonium Perchlorate-like Subsurface Decomposition

The formulation herein is quite similar to that of the foregoing section, and the same general assumptions are employed regarding uniformity of thermophysical properties and the high activation energy.

The following are exceptions: (1) The subsurface reaction is assumed of order zero with respect to its dependence upon the reactant concentration; this implies that the energy equation can be solved independently. (2) Melting and decomposition are intermingled, so that the "critical" temperature T_c (T_s) denotes herein both melting and the onset of reaction. Consequently (due to the high activation energy), one may expect

$$(T_c - T_s)/(T_s - T_0) \ll 1$$

(3) An appreciable extent of subsurface decomposition is expected, in contrast to the previous analysis for a nitramine-like substance.

A similar analysis was carried out by Cohen [A.1] and previously by Ramouhal and Cohen [A.2].

The energy equation for $\tau_c < \tau < 1$ is

$$(\tau - \phi)\, d\phi/d\tau = K_c^* e^{-f(\tau)/\varepsilon} \qquad (A.30)$$

where

$$\tau_c \equiv (T_c - T_0)/(T_s - T_0) \sim O(1)$$

The stretching transform of Eq. (A.14) can be applied again to the entire region; after neglecting terms of $O(\varepsilon)$, one obtains for

$$0 < \eta \equiv (1-\tau)/\varepsilon < \eta_c$$

the energy and species equations:

$$(1-\phi)\, d\phi/d\eta = -K_c^* e^{-\eta/a_1}, \quad \phi(\eta_c) = -q_m \qquad (A.31)$$

$$(1-\phi)\, dY/d\eta = +K_c\, e^{-\eta/a_1}, \quad Y(\eta_c) = 1 \qquad (A.32)$$

which obtain the solution

$$\phi(\eta) = 1 - \left[1 + q_m(2 + q_m) - 2 K_c^* a_1 e^{-\eta_c/a_1} \left(e^{-\frac{\eta_c - \eta}{a_1}} - 1 \right) \right]^{1/2}$$

$$(A.33)$$

Note that only the negative sign of the square root term has been retained [in the quadratic equation arising from solution of Eq. (A.31)] since at the surface, $\phi(0)$ is expected to be maximal.

The reference species (reactant) solution is similar

$$\Upsilon(\eta) = C - \phi(\eta) C_c (T_s - T_0)/Q_L^* \qquad (A.34a)$$

where C is a linear coupling constant, evaluated at the "cold" boundary:

$$C = 1 - q_m C_c (T_s - T_0)/Q_L^* = 1 - Q_m^*/Q_L^* \qquad (A.34b)$$

Now the values of the thermal gradient and the reactant mass fraction at the surface $\eta=0$ can be evaluated:

$$\mathbf{F} \equiv \tau'(0) = 1 - \phi(0) = \left[1 + q_m(2+q_m) + 2K_c^* a_1 (e^{-\eta_c/a_1} - 1) \right]^{1/2}$$

$$(A.35)$$

$$G = (1 - Q_m^*/Q_L^*) - \phi(0) C_c (T_s - T_0)/Q_L^* =$$

$$= \left[Q_L^* - Q_m^* - C_c(T_s - T_0) + C_c(T_s - T_0)\mathbf{F} \right]/Q_L^* \qquad (A.36)$$

where G is expected to depart appreciably from unity; for AP, $G \doteq 0.3$ is inferred. Furthermore, if G=const over a broad enough range of T_s (at fixed T_0), then in this range

$$(\partial G/\partial T_s)_{T_0} = 0$$

and, by Eq. (A.36), this condition leads to:

$$dF/dT_s = (1-F)/(T_s - T_0)$$

$$F \sim 1 - (T_R - T_0)/(T_s - T_0)$$

where T_R is a reference surface temperature, and the differential operator is defined

$$d/dT_s \equiv \partial/\partial T_s + (\partial m/\partial T_s) \, \partial/\partial m$$

All of these partial derivatives can be calculated from Eq. (A.35), since the (T_s, m)-dependences of each term are known explicitly, cf. Eqs. (A.4) - (A.7) and (A.10). Note that although G (T_s, m)=const for fixed T_0, one may still obtain for variable T_0

$$\delta G = (\partial G/\partial T_0) \, \delta T_0 \neq 0$$

80

The foregoing results have not been incorporated in the calculation of AP temperature sensitivity in the present study; i.e., G=const was assumed under all conditions. The major reason is the uncertainty involving T_c, the "critical" temperature (which might well be T_s-dependent to provide for G=const); without a clear physical definition of T_c, calculations would tend to be highly speculative.

It should be emphasized that $G(T_s, m; T_o ...)$=const=0.3 is in no way inferred in this study; it is imposed, according to indications made in the analysis of Guirao and Williams [32]. The detailed derivations of F and G in this section would be more useful for cases where G is variable, perhaps in simulation of the so-called foam zone in double base propellant deflagration.

References

A. 1   Cohen, N.S., "Analysis of Double-Base Propellant Combustion,"
       AIAA 19th Aerospace Sciences Mtg., Jan. 1981, Paper No.
       81-0120

A. 2   Cohen, N.S. et al,"Combustion Response Modeling for Composite
       Solid Propellants,"14th JANNAF Combustion Mtg., CPIA Publication
       292, vol. I, 1977, pp. 55-66.

APPENDIX B

SAMPLE CALCULATIONS AND DATUM POINTS –
COMPARISON WITH BDP MONOPROPELLANT

1.   BDP Calculations

The following formulation was used:

$$q = [C_c(T_s - T_o) - Q_s^*]/Q_f^* \qquad \text{(B.1)}$$

$$z_B = ln(1/q) \qquad \text{(B.2)}$$

$$m(T_s) = A_s \, exp(-\beta_s/T_s) \qquad \text{(B.3)}$$

$$K_1^o = (\lambda/C_p)K_1 \qquad \text{(B.4)}$$

$$p = \left(m^2/z_B K_1^o\right)^{1/n_1} \qquad \text{(B.5)}$$

For AP, the value of K_1^o was obtained by fitting a single experimental point (at $p = 4.5$ MPa, $m = 11.01$ kg/m^2-s), as follows: $T_s = 884.7$ k from Eq. (B.3)   and $z_B = 1.332$ from Eqs. (B.1) and (B.2); thus, from Eq. (B.5),

$$K_1^o(AP) = 9.619 \times 10^{-11} \quad (kg/m^2-s)^2 / Pa^{1.8}$$

Now, according to Eq. (B.4), using (λ/C_p) = 5 x 10^{-5} kg/m-s, one obtains

$$K_1(AP) = 1.924 \quad g/cc-s-atm^{1.8}$$

which is the kinetics constant for gas phase reaction, only slightly different from that of BDP, namely 1.12 g/cc-s-atm$^{1.8}$.

For HMX, a similar procedure (at p = 3 MPa, m = 11.33 kg/m^2-s) leads to T_s = 1133 K, Z_B = 3.288, and hence

$$K_1^o(HMX) = 4.339 \times 10^{-12} \; (kg/m^2\text{-}s)^2/Pa^2$$

In this case, using again $(\lambda/C_p) = 5 \times 10^{-5}$ kg/m-s, one finds from Eq. (B.4)

$$K_1(HMX) = 0.8678 \; g/cc\text{-}s\text{-}atm^2$$

which is somewhat larger than the value of 0.246 g/cc-s-atm^2 specified by BDP.

2. Present Model (MBR) Calculations

For AP, from the eigenvalue equation,

$$G = K_1 e^{-\beta_1/T_f} \; p^{n_1}/m^2 \qquad \text{(B.6)}$$

$$K_1 \equiv (\lambda/C_p)^o A_1^o / (R_u T_R/\overline{W})^{n_1} \qquad \text{(B.7)}$$

With the reference temperature taken T_R = 1000 K, and the reference-point data (p = 4.5 MPa, m = 11.01 kg/m^2-s), the value of K_1 can be calculated from Eq. (B.6) with G = 0.3 and T_f = 1400 K (for T_s = 873 K):

$$K_1(AP) = 1.387 \times 10^{-4} \; (kg/m^2\text{-}s)^2/Pa^{1.8}$$

Now, from Eq. (B.7), using $\lambda/C_p = 5 \times 10^{-5}$ kg/m-s and $\overline{W}$ = 30 g/mol,

$$A_1^o(AP) = 1.737 \times 10^{10} \; (kg/m^3\text{-}s)/(kg/m^3)^{1.8}$$

which is within an order of magnitude of the original Longwell-Weiss prefactor when converted to the proper units. The foregoing value of K_1 was used in the calculations of m, etc.

For HMX the strategy is slightly different and aimed to obtain first a value for n_1, the overall gaseous reaction order in the near field. The burning rate pressure sensitivity is written

$$n(p) = 0.5 \left[1 + 1/(1+B/p) \right] \qquad \text{(B.8)}$$

readily obtained from the HMX burning rate correlation 31,38

$$m = cp \left[1 + B/p \right]^{0.5}$$

with B = 3.84 MPa. This yields at the reference point (p = 3 MPa, m = 11.33 kg/m^2-s) n = 0.7193. From the pyrolysis formula, T_s = 683.3K and from Eqs. (28), G (T_s, m; T_o = 300 K) = 0.9265 and lg(G) $\cong$ -0.0764. The HMX pressure sensitivity formula is, explicitly:

$$n_1(p) = n \left[\left(\frac{T_s}{\beta_s} \cdot \frac{T_s - 2T_o}{T_s - T_o} + \frac{\beta_c}{\beta_s} - 2 \right) \ln G + 2 \right] \qquad \text{(B.9)}$$

using pertinent data from Table 2; thus

$$n_1(HMX) = 1.40$$

This result is in remarkable agreement with the computed value of n_1 = 1.3 in Ref. 38, where the upward shift from unity is explained by thermal enhancement, due to the presence of secondary reactions. Now, since T_f = constant in the present approximation, the eigenvalue equation obtains the constant factor,

$$K_1^o(HMX) = G m^2/p^{n_1} = 1.017 \times 10^{-7} \; (kg/m^2-s)^2/Pa^{1.4}$$

evaluated at the aforementioned reference point, with n_1 = 1.4; this value of K_1^o is used in the m vs p calculations herein. By definition,

$$K_1^o \equiv \left[\left(\frac{\lambda}{C_p} \right)^o A_1^o / (R_u T_R / \bar{w})^{n_1} \right] e^{-\beta_1/T_f}$$

where values of particular terms in the square brackets are unimportant. However, to facilitate comparison with the kinetics data (first order overall) of Shaw and Walker [39] , the mean temperature is taken at T_R = 1000 K, and a multiplicative factor of ρ^{n_1-1} is included to adjust the overall order; the prefactor is

$$A_1^\circ = K_1^\circ \, e^{-\beta_1/T_R} \left(p\bar{w}/R_u T_R \right)^{n_1} \Big/ \left[\left(\tfrac{\lambda}{c_p} \right)^\circ / \left(R_u T_R/\bar{w} \right)^{n_1} \right]$$

$$= 2.75 \times 10^{15} \; \text{1/sec}$$

with the foregoing values of K_1^0 , n, etc. This value is within an order of magnitude from 2.5×10^{16} 1/s specified by Shaw and Walker.

In summary, each of the models considered contains one overall kinetics parameter (or two, in the case of the present model for HMX), which was adjusted at a single experimental reference point (p, m). This adjustment is specific to the monopropellant simulated. For the present model, the adjusted parameters were shown to obtain kinetics prefactors in fair agreement with available chemical kinetics data.

NOMENCLATURE

A = pre-exponential factor, Arrhenius kinetics constant; 1/s for first order, m^3/mol-s for second order

C_p, C_c = specific heats for gas (isobaric) and condensed phase, respectively, J/kg-K

D = diffusion coefficient, gas mixture, m^2/s

E = activation energy, Arrhenius kinetics constant, kcal/mol

h = specific thermal enthalpy, J/kg

k_1, k_2 = reaction rate constant (Arrhenius form intended) for first order 1/sec, and for second order m^3/mol-s

M = total number of overall reactions in nonlinear gas phase model

m = mass burning rate, kg/m^2-s

N = total number of chemical species in gas phase model

n = burning rate pressure exponent in ap^n formula

p = pressure, MPa (Mega Pascal; 1 MPa = 10.013 atm)

Q = heat of reaction, J/mol (positive for exothermicity)

r = linear regression rate of burning propellant, m/s

q_s = surface heat balance parameter (representing liquid side)

R_u = universal gas constant, 1.987 cal/mol-K. In equation of state, MKS units used.

T = temperature, K

f   = final flame conditions

G, g   = gas phase property

i   = primary decomposition (i = 1) and
               secondary reactions (i = 2,...M)

j   = chemical species   (for j = 1,3...N-1)
               and thermal enthalpy   for j = N

L   = liquid phase

m   = property corresponding to melting

max   = maximal

s   = liquid-gas interface

sub   = sublimation

v   = vaporization property

0   = ambient conditions, e.g., initial solid
               phase temp. T_0.

Superscripts

$\tilde{(\ )}$ = dimensionless property

$\overline{(\ )}$ = mean property

*   = specific (per unit mass); in the melt
               layer analysis only: intrinsic phase
               property.

$(\ )^{+}$ = on the positive (or progressive
               coordinate) side of an interface

eq   = equilibrium

u = mean velocity of gas mixture, perpendicular to propellant surface, m/s

W = molecular weight, kg/mol

w_1, w_2 = primary and secondary reaction rates, respectively, $\text{mol/m}^3\text{-s}$

X = $\rho_B Y / \rho_c^*$, reduced liquid phase density fraction in melt layer

Y = mass fraction

y = length coordinate, m

z = dimensionless melt layer coordinate, Eq. (12)

ζ = dimensionless near field coordinate in the gas, defined by Eq. (22)

η = $\log(\zeta + C)$, dimensionless gas phase transform coordinate

λ = thermal conductivity, J/m-s-K

Λ = flame speed eigenvalue, based on maximal primary reaction rate

$\Delta y_j^{(i)} = (v_j'' - v_j')^i$ = net stoichiometric coefficient of j-th species in the i-th reaction; single and double primes denote reactant and product, respectively

ρ = mixture density, kg/m^3

τ = $(T-T_m)/(T_s-T_m)$ dimensionless melt layer enthalpy

ϕ = dependent variable in melt layer formulation, Eq. (16); also, in gas phase, Eq. (26)

ψ = V_g/V, porosity in the bubbly melt layer

Subscripts

B = bubbly melt layer, overall properties

c = condensed-phase property

DISTRIBUTION LIST

No. Of Copies	Organization	No. Of Copies	Organization
12	Administrator Defense Technical Info Center ATTN: DTIC-DDA Cameron Station Alexandria, VA 22314	4	Commander US Army Research Office ATTN: R. Girardelli D. Mann R. Singleton D. Squire Research Triangle Park, NC 27709
1	Commander USA DARCOM ATTN: DRCDMD-ST 5001 Eisenhower Avenue Alexandria, VA 22333	1	Commander USA Communications Research and Development Command ATTN: DRDCO-PPA-SA Fort Monmouth, NJ 07703
1	Commander USA ARRADCOM ATTN: DRDAR-TDC D. Gyorog Dover, NJ 07801	1	Commander USA Electronics Research and Development Command Technical Support Activity ATTN: DELSD-L Fort Monmouth, NJ 07703
2	Commander USA ARRADCOM ATTN: DRDAR-TSS Dover, NJ 07801	2	Commander USA ARRADCOM ATTN: DRDAR-LCA-G, D.S. Downs J.A. Lannon Dover, NJ 07801
1	Commander USA ARRCOM ATTN: DRSAR-LEP-L Rock Island, IL 61299	1	Commander USA ARRADCOM ATTN: DRDAR-LC, L. Harris Dover, NJ 07801
1	Director USA ARRADCOM Benet Weapons Laboratory ATTN: DRDAR-LCB-TL Watervliet, NY 12189	1	Commander USA ARRADCOM ATTN: DRDAR-SCA-T, L. Stiefel Dover, NJ 07801
1	Commander USA Aviation Research and Development Command ATTN: DRDAV-E 4300 Goodfellow Blvd. St. Louis, MO 63120	1	Commander USA Missile Command ATTN: DRSMI-R Redstone Arsenal, AL 35898
1	Director USA Air Mobility Research and Development Laboratory Ames Research Center Moffett Field, CA 94035	1	Commander USA Missile Command ATTN: DRSMI-YDL Redstone Arsenal, AL 35898
2	Commandant US Army Infantry School ATTN: ATSH-CD-CSO-OR Fort Benning, GA 31905		

DISTRIBUTION LIST

No. Of Copies	Organization
2	Commander USA Missile Command ATTN: DRSMI-RK, D.J. Ifshin Redstone Arsenal, AL 35898
1	Commander USA Tank Automotive Research and Development Command ATTN: DRDTA-UL Warren, MI 48090
1	Director USA TRADOC System Analysis Activity ATTN: ATAA-SL WSMR, NM 88002
1	Chief Naval Research ATTN: R.S. Miller, Code 432 800 N. Quincy Street Arlington, VA 22217
1	Navy Strategic Systems Project Office ATTN: R.D. Kinert, SP 2731 Washington, DC 20376
1	Commander Naval Air Systems Command ATTN: J. Ramnarace, AIR-54111C Washington, DC 20360
3	Commanding Officer Naval Ordnance Station ATTN: C. Irish S. Mitchell P.L. Stang, Code 515 Indian Head, MD 20640
1	Commander Naval Surface Weapons Center ATTN: J.L. East, Jr., G-20 Dahlgren, VA 22448
1	Commander Naval Surface Weapons Center ATTN: G.B. Wilmot, R-16 Silver Spring, MD 20910

No. Of Copies	Organization
4	Commander Naval Weapons Center ATTN: R.L. Derr, Code 388 China Lake, CA 93555
1	Commander Naval Weapons Center ATTN: T. Boggs China Lake, CA 93555
1	Commander US Naval Research Laboratory Washington DC 20375
1	Commanding Officer Naval Underwater Systems Center Weapons Dept. ATTN: R.S. Lazar/Code 36301 Newport, RI 02840
1	Superintendent Naval Postgraduate School Dept. of Aeronautics ATTN: D.W. Netzer Monterey, CA 93940
6	AFRPL (DRSC) ATTN: R. Geisler D. George B. Goshgarian J. Levine W. Roe D. Weaver Edwards AFB, CA 93523
1	AFATL/DLDL ATTN: O.K. Heiney Eglin AFB, FL 32542
1	AFOSR ATTN: L.H. Caveny Bolling Air Force Base Washington, DC 20332

DISTRIBUTION LIST

No. Of Copies	Organization	No. Of Copies	Organization
1	NASA Langley Research Center ATTN: G.B. Northam/MS 168 Hampton, VA 23365	2	Exxon Research & Engineering ATTN: A. Dean M. Chou P.O. Box 45 Linden, NJ 07036
4	National Bureau of Standards ATTN: J. Hastie M. Jacox T. Kashiwagi H. Semerjian Washington, DC 20234	1	Ford Aerospace and Communications Corp. DIVAD Division Div. Hq., Irvine ATTN: D. Williams Main Street & Ford Road Newport Beach, CA 92663
1	Aerojet Solid Propulsion Co. ATTN: P. Micheli Sacramento, CA 95813	1	General Electric Armament & Electrical Systems ATTN: M.J. Bulman Lakeside Avenue Burlington, VT 05402
1	Applied Combustion Technology, Inc. ATTN: A.M. Varney 2910 N. Orange Avenue Orlando, FL 32804	1	General Electric Company ATTN: M. Lapp Schenectady, NY 12301
2	Atlantic Research Corp. ATTN: M.K. King 5390 Cherokee Avenue Alexandria, VA 22314	1	General Electric Ordnance Systems ATTN: J. Mandzy 100 Plastics Avenue Pittsfield, MA 01203
1	Atlantic Research Corp. ATTN: R.H.W. Waesche 7511 Wellington Road Gainesville, VA 22065	1	General Motors Rsch Labs Physics Department ATTN: J.H. Bechtel Warren, MI 48090
1	AVCO Corporation AVCO Everett Rsch. Lab. Div. ATTN: D. Stickler 2385 Revere Beach Parkway Everett, MA 02149	3	Hercules Powder Co. Allegheny Ballistics Lab. ATTN: R.R. Miller P.O. Box 210 Cumberland, MD 21501
1	Battelle Memorial Institute Tactical Technology Center ATTN: J. Huggins 505 King Avenue Columbus, OH 43201	3	Hercules, Inc. Bacchus Works ATTN: K.P. McCarty P.O. Box 98 Magna, UT 84044
1	Calspan Corporation ATTN: E.B. Fisher P.O. Box 400 Buffalo, NY 14225		

DISTRIBUTION LIST

No. Of Copies	Organization	No. Of Copies	Organization
1	Hercules, Inc. AFATL/DLDL ATTN: R.L. Simmons Eglin AFB, FL 32542	1	Paul Gough Associates, Inc. ATTN: P.S. Gough P.O. Box 1614 Portsmouth, NH 03801
1	Honeywell, Inc. Defense Systems Division ATTN: D.E. Broden/ MS MN50-2000 600 2nd Street NE Hopkins, MN 55343	2	Princeton Combustion Research Laboratories ATTN: M. Summerfield N.A. Messina 1041 US Highway One North Princeton, NJ 08540
1	IBM Corporation ATTN: A.C. Tam Research Division 5600 Cottle Road San Jose, CA 95193	1	Pulsepower Systems, Inc. ATTN: L.C. Elmore 815 American Street San Carlos, CA 94070
1	Lawrence Livermore National Laboratory ATTN: C. Westbrook Livermore, CA 94550	1	Rockwell International Corp. Rocketdyne Division ATTN: J.E. Flanagan/HB02 6633 Canoga Avenue Canoga Park, CA 91304
1	Lockheed Missiles & Space Co. ATTN: George Lo 3251 Hanover Street Dept. 52-35/B204/2 Palo Alto, CA 94304	2	Sandia National Laboratories Combustion Sciences Dept. ATTN: R. Cattolica D. Stephenson Livermore, CA 94550
2	Los Alamos National Lab Center for Non-Linear Studies ATTN: B. Nichols L. Warner P.O. Box 1663 Los Alamos, NM 87545	1	Science Applications, Inc. ATTN: R.B. Edelman 9760 Owensworth Avenue Chatsworth, CA 91311
1	Olin Corporation Smokeless Powder Operations ATTN: R. L. Cook P.O. Box 222 St. Marks, FL 32355	1	Science Applications, Inc. ATTN: H.S. Pergament 1100 State Road, Bldg. N Princeton, NJ 08540
		1	Shock Hydrodynamics ATTN: W. Anderson 4710-16 Vineland Avenue North Hollywood, CA 91602
		1	Space Sciences, Inc. ATTN: M. Farber Monrovia, CA 91016

No. Of Copies	Organization	No. Of Copies	Organization
4	SRI International ATTN: S. Barker D. Crosley D. Golden Tech Lib 333 Ravenswood Avenue Menlo Park, CA 94025	1	Brigham Young University Dept. of Chemical Engineering ATTN: M.W. Beckstead Provo, UT 84601
1	Stevens Institute of Tech. Davidson Laboratory ATTN: R. McAlevy, III Hoboken, NJ 07030	2	California Institute of Tech. Jet Propulsion Laboratory ATTN: L.D. Strand/ MS 125/159 4800 Oak Grove Drive Pasadena, CA 91103
1	Teledyne McCormack-Selph ATTN: C. Leveritt 3601 Union Road Hollister, CA 95023	1	California Institute of Technology ATTN: F.E.C. Culick/ MC 301-46 204 Karman Lab. Pasadena, CA 91125
1	Thiokol Corporation Elkton Division ATTN: W.N. Brundige P.O. Box 241 Elkton, MD 21921	1	University of California, Berkeley Mechanical Engineering Dept. ATTN: J. Daily Berkeley, CA 94720
3	Thiokol Corporation Huntsville Division ATTN: D.A. Flanagan Huntsville, AL 35807	1	University of California Los Alamos National Lab. ATTN: T.D. Butler P.O. Box 1663, Mail Stop B216 Los Alamos, NM 87545
3	Thiokol Corporation Wasatch Division ATTN: J.A. Peterson P.O. Box 524 Brigham City, UT 84302	2	University of California, Santa Barbara Quantum Institute ATTN: K. Schofield M. Steinberg Santa Barbara, CA 93106
1	United Technologies ATTN: A.C. Eckbreth East Hartford, CT 06108	1	University of Southern California Dept. of Chemistry ATTN: S. Benson Los Angeles, CA 90007
2	United Technologies ATTN: R.S. Brown R.O. McLaren P.O. Box 358 Sunnyvale, CA 94086	1	Case Western Reserve Univ. Div. of Aerospace Sciences ATTN: J. Tien Cleveland, OH 44135
1	Universal Propulsion Company ATTN: H.J. McSpadden Black Canyon Stage 1 Box 1140 Phoenix, AZ 85029		

97

No. Of Copies	Organization	No. Of Copies	Organization
1	Cornell University Department of Chemistry ATTN: E. Grant Baker Laboratory Ithaca, NY 14853	1	University of Minnesota Dept. of Mechanical Engineering ATTN: E. Fletcher Minneapolis, MN 55455
1	Univ. of Dayton Rsch Inst. ATTN: D. Campbell AFRPL/PAP Stop 24 Edwards AFB, CA 93523	4	Pennsylvania State University Applied Research Laboratory ATTN: G.M. Faeth K.K. Kuo H. Palmer M. Micci University Park, PA 16802
1	University of Florida Dept. of Chemistry ATTN: J. Winefordner Gainesville, FL 32601	1	Polytechnic Institute of NY ATTN: S. Lederman Route 110 Farmingdale, NY 11735
3	Georgia Institute of Technology School of Aerospace Engineering ATTN: E. Price Atlanta, GA 30332	2	Princeton University Forrestal Campus Library ATTN: K. Brezinsky I. Glassman P.O. Box 710 Princeton, NJ 08540
2	Georgia Institute of Technology School of Aerospace Engineering ATTN: W.C. Strahle B.T. Zinn Atlanta, GA 30332	1	Princeton University MAE Dept., Eng. Quad. ATTN: F.A. Williams, D325 P.O. Box 710 Princeton, NJ 08540
1	Hughes Aircraft Company ATTN: T.E. Ward 8433 Fallbrook Avenue Canoga Park, CA 91303	2	Purdue University School of Aeronautics and Astronautics ATTN: R. Glick J.R. Osborn Grissom Hall West Lafayette, IN 47907
1	University of Illinois Dept of Mech Eng. ATTN: H. Krier 144 ME Bldg.,1206 W. Green St. Urbana, IL 61801	3	Purdue University School of Mechanical Engineering ATTN: N.M. Laurendeau S.N.B. Murthy D. Sweeney TSPC Chaffee Hall West Lafayette, IN 47906
1	Johns Hopkins University/APL Chemical Propulsion Information Agency ATTN: T.W. Christian Johns Hopkins Road Laurel, MD 20707		

DISTRIBUTION LIST

No. of Copies	Organization
1	Rensselaer Polytechnic Inst. Dept. of Chemical Engineering ATTN: A. Fontijn Troy, NY 12181
2	Southwest Research Institute ATTN: Robert E. White A.B. Wenzel 8500 Culebra Rd. San Antonio, TX 78228
1	Stanford University Dept. of Mechanical Engineering ATTN: R. Hanson Stanford, CA 94305
2	University of Texas Dept. of Chemistry ATTN: W. Gardiner H. Schaefer Austin, TX 78712
1	University of Utah Dept. of Chemical Engineering ATTN: G. Flandro Salt Lake City, UT 84112
1	Virginia Polytechnical Institute State University ATTN: J.A. Schetz Blacksburg, VA 24061

Aberdeen Proving Ground

Dir, USAMSAA
  ATTN: DRXSY-D
        DRXSY-MP, H. Cohen
Cdr, USATECOM
  ATTN: DRSTE-TO-F
Dir, USACSL, Bldg. E3516, EA
  ATTN: DRDAR-CLB-PA
        DRDAR-CLN
        DRDAR-CLJ-L

USER EVALUATION OF REPORT

Please take a few minutes to answer the questions below; tear out this sheet, fold as indicated, staple or tape closed, and place in the mail. Your comments will provide us with information for improving future reports.

1. BRL Report Number_____

2. Does this report satisfy a need? (Comment on purpose, related project, or other area of interest for which report will be used.)

_____

_____

_____

3. How, specifically, is the report being used? (Information source, design data or procedure, management procedure, source of ideas, etc.)_____

_____

_____

4. Has the information in this report led to any quantitative savings as far as man-hours/contract dollars saved, operating costs avoided, efficiencies achieved, etc.? If so, please elaborate.

_____

_____

5. General Comments (Indicate what you think should be changed to make this report and future reports of this type more responsive to your needs, more usable, improve readability, etc.)_____

_____

_____

_____

6. If you would like to be contacted by the personnel who prepared this report to raise specific questions or discuss the topic, please fill in the following information.

               Name:_____

    Telephone Number:_____

Organization Address:_____

                     _____

                     _____